The Response of the Northwest Atlantic Ocean to Climate Change

Michael A. Alexander[1], Sang-ik Shin[1,2], James D. Scott[1,2], Enrique Curchitser[3], Charles Stock[4]

1 - NOAA/Earth System Research Laboratory, Boulder, Colorado
2 - Cooperative Institute for Research in Environmental Sciences, University of Colorado Boulder, Boulder, Colorado
3 - Department of Environmental Sciences, Rutgers, The State University of New Jersey, New Brunswick, New Jersey
4 - NOAA/Geophysical Fluid Dynamics Laboratory, Princeton, New Jersey

Manuscript submitted to the Journal of Climate, February 2019

Corresponding Authors Address:
Michael Alexander
NOAA, Earth System Research Laboratory
R/PSD1
325 Broadway
Boulder, CO 80305-3328
Michael.Alexander@noaa.gov

Abstract

ROMS, a high-resolution regional ocean model, was used to study how climate change may affect the northwest Atlantic Ocean. A control (CTRL) simulation was conducted for the recent past (1976-2005), and simulations with additional forcing at the surface and lateral boundaries, obtained from three different global climate models (GCMs) using the RCP8.5 scenario, were conducted to represent the future (2070-2099). The climate change response was obtained from the difference between the CTRL and each of the three future simulations.

All three ROMS simulations indicated large increases in sea surface temperatures (SSTs) over most of the domain except off the eastern US seaboard due to weakening of the Gulf Stream. There are also substantial inter-model differences in the response, including a southward shift of the Gulf Stream in one simulation and a slight northward shift in the other two, with corresponding changes in eddy activity. The depth of maximum warming varied among the three simulations, resulting in differences in the bottom temperature response in coastal regions, including the Gulf of Maine and the west Florida Shelf. The surface salinity decreased (increased) in the northern (southern) part of the domain in all three experiments, but in one, the freshening extended much further south in ROMS than in the GCM that provided the large-scale forcing, associated with changes in the well resolved coastal currents. Thus, while high resolution allows for a better representation of currents and bathymetry, the response to climate change can vary considerably depending on the large-scale forcing.

1. Introduction

The increase in greenhouse gasses over the past century has contributed to the warming of most of the world's oceans, including highly productive coastal regions responsible for the vast majority of global fish catch (e.g. Pauly and Zeller 2016). For example, Belkin (2009) found that 61 of the 63 large marine ecosystems (LMEs) that are mainly located in coastal regions exhibited warming from 1982–2006, while Lima and Wethey (2012) found that ~3/4 of coastal areas experienced an increase in SST, with an overall rate of 0.25°C dec^{-1}, from 1982 to 2010. While broad warming due to accumulating greenhouse gasses is likely to continue, these trends may be significantly exacerbated (or ameliorated) by regional processes such as the retreat of sea ice, changes in finer-scale features, such as fronts and eddies, and the effects of small-scale coastal/bathymetric features on the response to climate change. Given that complex ocean current systems and highly productive marine ecosystems are often located near land, where climate change induced warming is expected to be more intense, greenhouse gas induced changes may have an especially pronounced effects in coastal areas. This could well be the case for the US east coast and Gulf of Mexico, given the proximity of the Labrador Current, Gulf Stream, and Loop current, and complex bathymetric features such as the Laurentian Channel, Gulf of Maine, Georges Bank and west Florida Shelf (Fig. 1). Climate change will not only influence SST but also temperature, salinity and currents throughout the water column, which can subsequently impact marine ecosystems. Thus, models and datasets with high spatial resolution may be necessary to fully diagnose and simulate the effects of climate change in the northwest Atlantic and Gulf of Mexico.

Consistent with the potential for regional dynamics to shape large-scale warming patterns, observational analyses indicate a range in SST trends along the east coast of North America.

Belkin (2009) found moderate to strong warming for the Scotian Shelf, moderate warming in the Gulf of Mexico and modest warming on the NE and SE US shelf between 1982 and 2006, although the warming was quite strong for the NE US over the longer period of 1957-2006. Analyses of observations directly adjacent to the coast suggest weak cooling in the southeast and somewhat stronger warming for the northeast US coast (Shearman and Lentz 2010, Lima and Wethey 2012), where Gulf of Maine SST increased by more than 2°C between 2004 and 2013, nearly the largest increase over the global ocean during that period (Pershing et al. 2015).

Large changes are also projected for the North Atlantic Ocean in the future. Alexander et al. (2018) found that SSTs increase by approximately 0.3°-0.4° C dec^{-1} over the period 1976-2099 for LMEs along the US east coast with even stronger warming of 0.5°C dec^{-1} on the Scotian Shelf based on simulations using the Representative Concentration Pathway 8.5 (RCP8.5) scenario from phase 5 of the Coupled Models Intercomparison Project (CMIP5) archive. The very strong warming over the high latitude continents and the Arctic Ocean, i.e. polar amplification, and the reduction in sea ice, likely contributes to changes over the Atlantic through both the atmosphere and the ocean (e.g. Pedersen et al. 2016, Chen et al. 2014, Coumou et al. 2018, Sun et al. 2018). In general, the models indicate that ocean warming is greatest near the surface, which enhances the static stability, as does the surface freshening of the Atlantic north of ~45°N (Capotondi et al. 2012). The enhanced stratification, particularly at high latitude regions in the North Atlantic, reduces convection and slows the Atlantic meridional overturning circulation (AMOC, e.g. Cheng et al. 2013; Collins et al. 2013). In turn, changes in AMOC influence temperature and salinity (Drijfhout et al. 2012). In the CMIP5 models, a decrease in AMOC is associated with cooling south of Greenland ("warming hole"), warming southeast of Nova Scotia, decreased salinity in the subpolar gyre, and

91 increased salinity in the subtropical gyre, especially near the southeast US coast (Cheng et al.
92 2013). Changes in AMOC have the potential to alter basin-wide circulation patterns that impact
93 the physical/biological ocean response of the east coast of North America.

94 The resolution of the GCMs used in CMIP5 is relatively coarse, with an ocean resolution
95 on the order of 100 km, which does not resolve fine-scale topographic features and may not
96 adequately represent aspects of the ocean dynamics. For example, these models do not resolve
97 ocean eddies and simulate the separation of the Gulf Stream from the coast north of its observed
98 location at Cape Hatteras (e.g. Bryan et al. 2007), which can influence the response to
99 increasing greenhouse gasses (Winton et al. 2014). Saba et al. (2016) investigated the response
100 of GCMs developed at the NOAA Geophysical Fluid Dynamics Laboratory (GFDL) with
101 varying atmosphere and ocean resolutions to a doubling of CO_2 (after an increase of 1% per
102 year). They found that the response to climate change varied with resolution, especially along
103 the northeast US coast, where the increase in temperature was much stronger in the simulation
104 with the finest resolution: 50 km in the atmosphere and 10 km in the ocean. At this resolution,
105 the SST warming off portions of the east coast exceeded 5°C, ~2.5 times greater than the
106 increase in the global mean and double that of the coarse resolution GCM. The warming was
107 especially strong in the Gulf of Maine, where very warm water from the Atlantic entered the
108 Gulf at depth through the northeast channel, which was only resolved in the highest resolution
109 simulation. The surface salinity increased along the most of the US east coast shelf, with strong
110 increases in bottom salinity along the North and South Carolina coast, and into the Gulf of
111 Maine and Scotian shelf via deep channels. Saba et al. (2016) attributed these changes in
112 temperature and salinity to a decrease in AMOC and a northward shift of the Gulf Stream.

While the projected changes in the Atlantic temperature, salinity and currents are generally consistent with those observed to date (e.g. Boyer et al. 2005, Wu et al. 2012, Knutson et al. 2013, Ceaser et al. 2018), both the observed and simulated changes could reflect decadal climate variability. In addition, there are large differences between models in their representation of AMOC, other atmospheric and ocean processes, and their response to climate change (e.g. Gregory et al. 2005, Danabasoglu 2008, Cheng et al. 2013, Karspeck et al. 2017), and even small differences in the basin-scale response to climate change could result in large differences in coastal regions. Thus, while the high-resolution GCM study of Saba et al. (2016) is very informative, it is based on a highly idealized CO_2 scenario and represents just one potential future for the North Atlantic Ocean. Since high-resolution global models are very computationally intensive, an alternative approach is to dynamically downscale the large-scale changes obtained from the GCM simulations using regional ocean models forced by GCM output along their open ocean lateral boundaries and at the surface. Usually the GCM forcing is bias corrected, removing the mean difference between the model and observations in the historical period. Dynamically downscaled climate change simulations have been conducted for several regions including the California Current System (Auad et al., 2006, Xiu et al. 2018), the Bering Sea (Hermann et al. 2016), western North Pacific (Liu et al. 2016), Australian boundary currents (Sun 2012) and the Caribbean/Gulf of Mexico (Liu et al. 2012, van Hooidonk et al. 2015; Liu et al. 2015). The regional model studies of the Gulf of Mexico indicate weakening of the Loop Current and associated warm transient eddies, which reduces the amount of anthropogenic warming especially in spring, while surface heating leads to intense warming on the northeastern shelf in summer (Liu et al. 2015). The experiments

conducted by Liu et al. (2012, 2015), however, used a multi-GCM mean to drive a regional ocean model, thereby retaining only the linear component of the climate change forcing.

Here we force the same regional model using fields from three different GCMs, enabling us to generate a range of responses and test their robustness. We also examine a wide range of variables including SST, bottom temperature, surface and bottom salinity, static stability, currents and eddies, over much of the northwest Atlantic, from the western Caribbean Sea to the Gulf of Saint Lawrence. We present the results for December-January-February (DJF) and June-July-August (JJA), since the energetics of the Gulf Stream is seasonally dependent (Kang et al. 2016) and the response to climate change can differ between winter and summer (e.g. Alexander et al. 2018). The model and experiment design are described in section 2, the findings from the regional model are presented in section 3 and the results are summarized and discussed in section 4.

2. Models and Methods

a. Regional Ocean Model

We used the Regional Ocean Modeling System (ROMS, Shchepetkin and McWilliams 2003, 2005) to investigate the effects of climate change on the northwest Atlantic. ROMS is a terrain-following primitive equation model with a free surface using incompressible and hydrostatic approximations. The version used here, configured by Kang and Curchitser (2013), has a horizontal grid spacing of 7 km and 40 vertical sigma levels with higher resolution near the surface. The domain extends along the east coast of North America from approximately 10°N to 52°N, covering the western Caribbean, Gulf of Mexico, and the western North Atlantic from Florida to Newfoundland and includes the Loop Current, Florida Current, Gulf Stream

158 and the southern portion of the Labrador current (Fig. 1). The initial and oceanic boundary
159 forcing for the control (**CTRL**) ROMS simulation is based on 5-day averages from the Simple
160 Ocean Data Assimilation (SODA v2.1.6; Carton and Giese 2008), 6-hourly surface forcing
161 from the Co-ordinated Ocean–Ice Reference Experiments (CORE v2; Large and Yeager 2009)
162 and daily fresh water flux from rivers from the continental discharge data base (Dai et al. 2009).
163 The CTRL simulation is performed using the observed forcing over a 48-year period: 1958-
164 2005. The mean path of the Gulf Stream and the associated distribution of eddy kinetic energy
165 simulated by this configuration of ROMS is in good agreement with observations (Kang and
166 Curchitser 2013, 2015; Chen et al. 2018).
167
168 *b. Climate change simulations – "Delta Method"*
169 The large-scale climate change forcing is implemented using the "delta method", where
170 the difference between *mean* conditions from a future and a recent period are added to
171 observations that vary with time during the recent period. Since the recent periods mean
172 climate and high-frequency variability is retained from observations, this method removes the
173 mean bias and retains realistic unforced climate variability over a range of time scales.
174 However, the imposed climate change signal at the boundaries is still at a coarse resolution, it
175 does not allow for a change in variability in the future, and it assumes that the mean climate
176 state and the projected change are not highly correlated, i.e. the bias is not strongly dependent
177 on the mean climate state (e.g., Hare et al. 2012). Here, the delta (Δ) values were obtained by
178 subtracting the mean values during 1976-2005 from those in 2070-2099, where the future
179 period is simulated based on RCP8.5, representing the "business-as-usual" scenario assuming
180 little to no stabilization of greenhouse gas emissions by 2100. Since a key aspect of this study

is to perform a comprehensive analysis of multiple models, which is computationally intensive, we chose to use the RCP8.5 scenario as it has the greatest increase in greenhouse gases in IPCC AR5, and thus should have the largest signal-to-noise ratio.

The Δs were computed for each calendar month and then interpolated to daily values, which were then added to the observed forcing and initial ocean conditions in the CTRL. Like the CTRL, the **RCP8.5** (CTRL + Δforcing) ROMS simulations are 48 years long. The ROMS response to the inclusion of GCM forcing is obtained from the average of the RCP8.5 - CTRL values over the last 30 years (1976-2005 in the CTRL) of the simulation, allowing the model time (18 years) to spin-up to the additional forcing.

The surface fields from the GCMs needed to drive ROMS include near surface air temperature and humidity, evaporation – precipitation (E-P), sea level pressure (SLP), zonal and meridional winds, and the downwelling radiation at the surface. The necessary ocean fields include sea surface height and temperature, salinity, zonal (u) and meridional (v) currents as a function of depth. Freshwater flux Δs into the ocean from major rivers are applied at the locations identified in the Dai et al. 2009 data base.

The initial conditions and boundary forcing Δs were obtained from three GCMs used in the fifth IPCC assessment: the GFDL ESM2M, Institute Pierre Simon Laplace (IPSL) CM5A-MR, and the Hadley Center HadGem2-CC. These three models were chosen in part due to their differences in AMOC in both their climatology and response to anthropogenic forcing. In addition, they are earth system models and thus could provide the necessary forcing fields in future downscaling experiments that include biogeochemistry. The resolution, transient climate response as indicated by the increase in global air temperature, and the climatological and Δ AMOC values for the three models are provided in Table 1..

3. Results

a Temperature

The SST response to projected climate change (RCP8.5 – CTRL, shading in Fig. 2) includes warming over nearly the entire domain in both winter (DJF) and summer (JJA) for the three GCM-driven ROMS simulations that are subsequently referred to as GFDL-ROMS, IPSL-ROMS and HadGEM-ROMS. The warming is lessened in and to the south of the Gulf Stream front, as indicated by the region of strong temperature gradients (contours from the CTRL in Fig. 2), especially during DJF in all three ROMS simulations. This reduced warming is primarily due to changes in the meridional ocean heat transport. As the Gulf Stream slows in the future (see section 3e), i.e. the response opposes the mean current, it transports less heat northward off the southeast US coast (Fig. 1 in the Supplementary Material, Fig. SM1). From a heat budget perspective, the change in the surface currents times the mean SST gradient is negative, which acts to cool the SSTs (Fig. SM1 bottom). While this process occurs in all three simulations, it is especially strong in the GFDL-ROMS experiment. During summer a strong shallow mixed layer forms and the surface layer is decoupled from the deeper ocean and reflects stronger thermodynamic air-sea coupling, reducing the effects of the change in heat transport on SST.

There are other notable differences among the three simulations. The IPSL-ROMS and HadGEM-ROMS simulations exhibit very strong warming (> 4°C) in the northwest part of the domain, while the warming in GDFL-ROMS is on the order of 2°C. Enhanced coastal warming relative to adjacent ocean waters is far more extensive in the HadGEM-ROMS simulation than in the other models during winter, when it extends along the nearly the entire US coast and

227 into Canadian waters. The simulations, especially GFDL-ROMS and HadGEM-ROMS,
228 indicate very strong warming on the outer west Florida shelf during winter; while Liu et al.
229 (2015) also found enhanced warming in this region, it occurred on the inner shelf in summer.
230 The broad structure of the three SST responses in ROMS are driven by the basin-scale
231 changes as can be seen by relating the ROMS response to the changes in the corresponding
232 GCM. For example, like the ROMS simulations, the global models indicate reduced warming
233 in the Gulf Stream region and its extension into the North Atlantic (with a corresponding
234 decrease in the currents, section 3.e), especially in the GFDL GCM during winter (Fig. SM2).
235 The three GCMS also indicate intense warming of the surface air temperature over eastern
236 Canada especially in winter (Fig. 3), partly due to a reduction in sea ice and snow cover in and
237 around Hudson Bay. The mean winds from the west (Fig. 3) can transport the additional heat
238 over the adjacent ocean, where increased air temperature warms the underlying ocean via the
239 surface heat fluxes, especially near the coast. The increase in air temperature over North
240 America corresponds to the overall climate sensitivity of these three GCMs, which is relatively
241 weak, moderate and strong, in the GFDL, IPSL and HadGEM GCMs (Table 1, Fig. 3),
242 respectively, as are the increases in SST off the coast of the northeast US and southern Canada
243 in the GCMs (Fig. SM2) and the corresponding ROMS simulations (Fig. 2).
244 There are also clear differences between the downscaled simulations and the corresponding
245 GCMs which drove them. In the GFDL and IPSL experiments, the downscaled simulation
246 exhibits less warming in the Gulf Stream region compared to the GCM, while for HadGEM,
247 the ROMS simulation generally exhibits less warming over much of the domain except along
248 portions of the eastern seaboard relative to the driving GCM. Differences between the global
249 and regional SST responses to anthropogenic forcing reached 2°C in some locations.

The bottom temperature (BT) response in all three downscaled experiments indicates warming along the entire continental shelf in both DJF and JJA (Fig. 4). They also indicate enhanced warming over portions of maritime Canada, on the shelf in the Gulf of Mexico, and in a narrow band along the shelf break (in the vicinity of the 200 m isobath) off the southeast US coast in summer. The increase in bottom temperature in coastal regions is often greater than at the surface in all three simulations. For example, the increase in SST during JJA over the west Florida shelf is on the order of 2.5°C but for BT it exceeds 3.5°C in all three ROMS simulation. There are also substantial differences in the detailed BT structure among the three ROMS simulations, which are clearly influenced by both the large-scale forcing and small-scale topographic features (compare Figs. 4 and SM3). Like SST, the strongest increase in BT (> 4°C) occurs over a broad region north of Cape Hatteras in HadGEM-ROMS. At regional scales, which are not resolved by the GCMs, a strong BT response occurs in the Laurentian Channel that extends from the shelf break to the mouth of the Saint Lawrence River in GFDL-ROMS. In contrast, the strongest increase in BT in IPSL-ROMS and HadGEM-ROMS is not in the bottom of the Channel, but in shallower portions of the Gulf of Saint Lawrence and on the shelf off the coast of Newfoundland and Nova Scotia.

b. Salinity

The sea surface salinity (SSS) response in ROMS for the three forcing experiments is shown for DJF and JJA in Fig. 5. The SSS values exhibit decreased salinity in the northwest corner of the domain in both summer and winter. Like the ROMS simulations, the large-scale salinity changes in the original GCM simulations indicate a decrease in salinity north of ~40°N (Fig. SM4), partly due to increased net surface freshwater flux into the ocean; i.e. Δ(E-P) is

generally negative with large amplitude over the center of the subpolar gyre and the southern Labrador Sea (Fig. SM5), but more regional E-P changes vary in magnitude, location and by season among the three GCMs. Since the largest response in E-P and the melting of sea ice primarily occur outside of the ROMS domain, the decrease in salinity off the New England and Canadian coast is likely due to advection of fresher water into the region. The salinity increase south of 40°N, is generally consistent with where Δ(E-P)>0.

Notable differences in SSS occur along the northeast US coast among the three ROMS simulations and between the individual ROMS simulations and the GCMs that drove them. The southward extent of enhanced freshening along the coast of North America is greatest in GFDL-ROMS, where it extends to North Carolina, while it is primarily confined to Canadian waters in DJF and north of New Jersey in JJA in IPSL-ROMS and HadGEM-ROMS. The freshening along the northeast coast also extends further south in GFDL-ROMS than in the GFDL GCM itself, while the reverse is true in the IPSL and HADGEM experiments. The salinity response may reflect advection by changes in the well-resolved downscaled currents, although changes in other processes such as river runoff, stratification, eddy mixing, etc., could influence the detailed structure of the SSS changes.

The salinity changes in the southern portion of the domain are consistent with enhanced evaporation relative to precipitation in the future climate (Δ(E-P) > 0) over most of the Atlantic south of ~40°N and the Gulf of Mexico in all three GCMs (Fig. SM5). However, there are differences between where Δ(E-P) is large and the location and amplitude of the SSS response in the ROMS simulations and the corresponding GCMs in portions of the Gulf of Mexico. This difference is especially notable in the northern Gulf of Mexico in the HadGEM experiment, where ΔE-P is positive and the SSS slightly increases in the GCM but decreases in HadGEM-

296 ROMS. Freshwater entering the Gulf from the Mississippi River is greatly enhanced in the
297 HadGEM GCM (Fig. SM6) resulting in SSS decreases in the future in HadGEM-ROMS
298 simulations especially in JJA (Fig. 5). Higher vertical and horizontal resolution in conjunction
299 with reduced diffusion coefficients in ROMS relative to the coarse GCMs can act to maintain
300 fine-scale features, such as river plumes. While the SSS generally increases in the other two
301 ROMS simulations in the Gulf of Mexico, the change is smaller in northern portions of the
302 basin in JJA, where changes in currents and stratification may also play a role in the detailed
303 pattern of the response.

304 The response to climate change in the bottom salinity in the three ROMS simulations is
305 shown during DJF and JJA in Fig. 6 (and in Fig. SM7 for the GCMs). They have the same
306 general structure as those at the surface over most of the domain, although the magnitude and
307 extent of the changes tend to be smaller at the bottom. However, the response is very different
308 in the Laurentian Channel where the water becomes saltier on the bottom while it is freshening
309 at the surface. The apparent change in the salinity with depth is readily apparent in GFDL-
310 ROMS, where the bottom salinity increases in the Laurentian Channel (depth > 200 m) but
311 decreases nearly everywhere else north of Nova Scotia.

312

313 *c. Cross sections*

314 The structure of the vertical temperature and salinity changes in the three ROMS
315 integrations is explored further using cross sections in the vicinity of the Laurentian
316 Channel/Gulf of Saint Lawrence, Northeast Channel/Gulf of Maine and across the northern
317 Gulf of Mexico (see Fig. 1a). Note that the first two sections follow the maximum depth in
318 their respective channels and therefore they do not follow a fixed latitude or longitude. Since

319 the cross sections are qualitatively similar in DJF and JJA, we present the annual mean values
320 for the CTRL (contours) and the RCP8.5-CTRL (shading).

321 In the Gulf of Saint Lawrence, there is a temperature minimum at ~40 m depth and a
322 vertical front near the Atlantic-Gulf boundary at ~45ºN in the 30-year climatology from the
323 CTRL simulation (Fig. 7, top panels). While warming occurs throughout the Laurentian
324 Channel, the temperature departures are largest at depth in GFDL-ROMS (Fig. 7a), while the
325 maximum departures extend from near the surface to about 250 m in the other two simulations
326 (Fig. 7b,c). The maximum downscaled warming exceeds 3.5ºC in the GFDL and IPSL, and
327 5ºC in HadGEM. All three ROMS simulations indicate freshening of the surface layer,
328 extending to approximately 100, 75 and 50 m depth in the GFDL, HadGEM and IPSL
329 experiments, respectively, but the magnitude of the response is substantially smaller in IPSL-
330 ROMS (Fig. 7, bottom). All three simulations also have an increase in salinity at depth in the
331 Gulf of Saint Lawrence, which slopes downward from the southeast to the northwest.

332 The Gulf of Maine section (Fig. 8), includes the Northeast Channel (66°W), Georges Basin
333 (67°W) and Wilkinson Basin (69.5°W). In the CTRL, there is a strong vertical thermohaline
334 front near the entrance to the Gulf of Maine around ~65.5°W with colder and fresher water in
335 the Gulf relative to the Atlantic. The strongest warming in GFDL-ROMS is located at depths
336 below ~130 m in the open ocean (east of 65.5°W), which extends into Georges Basin through
337 the Northeast Channel (Fig. 8a). In the other two simulations (Fig. 8 b,c), the warming occurs
338 higher in the water column, where the temperature departures exceed 5°C in HadGEM-ROMS
339 at ~60 m depth at ~67.5°W. While salinity is enhanced in all three simulations in the Atlantic,
340 the overall response strongly differs between them (Fig. 8 bottom panels). The most notable
341 difference occurs in the surface layer in the Gulf of Maine where GFDL-ROMS exhibits

freshening while the salinity increases in IPSL-ROMS and to a lesser degree in HadGEM-ROMS. In the open ocean, the salinity increases by more than 0.4 PSU at depths greater than ~150 m in GFDL-ROMS, while the changes are slightly smaller and occur higher in the water column in the two other simulations. Only a small amount of the saltier water extends into the Gulf of Maine, likely advected through the northeast channel in the GFDL-ROMS, resulting in slightly saltier water below ~200 m in Georges Basin. In IPSL-ROMS, a layer with enhanced salinity penetrates eastward over the entire Gulf of Maine, with a maximum at ~50 m within the climatological halocline but also with salty water penetrating to the bottom of Georges Basin. HadGEM-ROMS is somewhere between the two other experiments, where the increase in salinity also slopes downward into Georges Basin, with a weak response above 50 m.

The temperature and salinity changes differ between the surface and the bottom in the northern Gulf of Mexico (sections 3a&b), indicating vertical structure in the response to climate change; thus, we present a zonal section along 28°N between the central coasts of Florida and Texas (Fig. 9). The CTRL exhibits a steady decrease in temperature with depth with a maximum gradient from around 40 to 150 m, where the thermocline is stronger and shallower near the coasts. The salinity in the CTRL exhibits much less vertical structure, but has a broad maximum over approximately 85°-93°W, with much fresher water near the coasts. In all three ROMS simulations, the temperature change is positive over the full width and depth of the Gulf of Mexico and is larger at depths between approximately 40-150 m than at the surface (Fig. 9 top panels), though the warming is slightly greater and most extensive in GFDL-ROMS. The response is enhanced where the thermocline intersects the west Florida Shelf at ~85°W, especially in GFDL-ROMS and HadGEM-ROMS, where it reaches 5°C, in line with the strong increase in bottom temperature on the west Florida Slope (Fig. 4). The respective

365 increases in salinity are relatively strong, moderate and weak in the downscaled GFDL, IPSL,
366 HadGEM simulations, respectively (Fig. 9 bottom panels). The changes are largest near the
367 Florida Coast in GFDL-ROMS and HadGEM-ROMS and near the Texas Coast in the shallow
368 climatological halocline in all three ROMS integrations. The salinity responses are also
369 enhanced across the entire basin between approximately 40 and 100 m depth in IPSL-ROMS
370 and HadGEM-ROMS; there is a slight increase at depth in GFDL-ROMS but it does not extend
371 across the basin.
372
373 *d. Density*
374 The depth dependent changes in temperature and salinity alter the density profile and thus
375 stratification. Stratification, as indicated by the density difference between 100 m depth and
376 the surface, is positive for stable stratification. The changes in stratification are shown for the
377 three ROMS simulations during DJF and JJA in Fig. 10. With intensified surface warming in
378 the future most of the open ocean areas of the North Atlantic in all three ROMS simulations
379 display an increase in stratification particularly in summer, consistent with Capotondi et al.
380 (2012) and Alexander et al. (2018). However, in the Gulf Stream region and in the Gulf of
381 Mexico the response is more complex. There is a decrease in stratification in the Gulf Stream
382 near the coast and a near-neutral response as it leaves the coast near Cape Hatteras and extends
383 into the Atlantic (where it is a minimum in the CTRL) during winter. Off the southeast US
384 coast, the weakening of the Gulf Stream is greater at the surface than at depth (discussed in the
385 following section) and there is intensified warming adjacent to the shelf break both of which
386 may enhance warming at depth relative to the surface. The stratification actually decreases
387 over nearly all of the Gulf of Mexico in GFDL-ROMS and IPSL-ROMS and in the center of

388 the Gulf in HadGEM-ROMS during DJF. In the Gulf, warming at depth is greater than at the
389 surface, leading to a negative change in the thermodynamic component of stratification (SST
390 - T_{100m}) in the downscaled simulations (Fig. SM8), especially when compared with the original
391 GCM simulations, which indicate enhanced stratification (Fig. SM9) due to an increase in (SST
392 - T_{100m}; Fig. SM10). The stratification changes vary among the three ROMS simulations over
393 the Gulf of Mexico during JJA (Fig. 10), but all three exhibit decreased stratification in the
394 east-central part of the basin (~25°N, 87°W).
395
396 *e. Currents*
397 A clear result in all three ROMS simulations is the weakening of the western boundary
398 current system over the entire domain including the Yucatan, Loop, and Florida Currents and
399 the Gulf Stream in both winter and summer (Fig. 11). The three forcing GCMs also show a
400 weakening of the western boundary current system in the western North Atlantic, although the
401 reduction in current strength in the IPSL GCM (Fig. SM11) is smaller than in IPSL-ROMS.
402 The weakening of the currents is especially pronounced in the Gulf Stream, whose speed
403 decreases by more than 25% in the three ROMS simulations relative to the CTRL, as indicated
404 by a cross section of the meridional velocity at 30ºN (Fig. 12). A more detailed map of the
405 annual mean surface currents off the NE US coast for the CTRL and the response to climate
406 change in three ROMS experiments are shown in Fig. 13. The response in GFDL- ROMS
407 simulation opposes the mean Gulf Stream flow in the center and northern part of the current
408 with a weak enhancement on its southern flank. This is highlighted in a meridional cross
409 section of the zonal current at 70ºW (Fig. 14a) indicating a southward displacement of the
410 current where the Gulf Stream is mainly zonal. The response in IPSL-ROMS and HadGEM-

411 ROMS exhibit an anomalous anticyclonic (clockwise) gyre starting near Cape Hatteras, where
412 the current separates from the coast, to the south of Long Island (~72ºW, Fig. 13c) in IPSL-
413 ROMS and Cape Cod (~65ºW, Fig. 13d) in HadGEM-ROMS. This feature weakens the
414 northern core of the Gulf Stream but enhances northeasterly flows along its northern edge
415 (Figs. 11,13). The latter aspect of the response is consistent with Saba et al. (2016), who found
416 enhanced meridional flow nearshore (~36ºN, 74ºW) and a northward shift of the current.
417 However, the enhanced flow on the northernmost edge of the Gulf Stream remains south of
418 ~40ºN and west of the Gulf of Maine in both IPSL-ROMS and HadGEM-ROMS (Figs. 11, 13,
419 14). In addition, the response in all three ROMS simulations indicates that water enters the
420 Gulf of Maine from the east along the Scotian Shelf and then flows counterclockwise around
421 the basin. This enhances the mean circulation at the surface (Fig. 13) and at depths down to
422 200 m (as can be displayed at https://www.esrl.noaa.gov/psd/ipcc/roms/roms.html). Thus, the
423 responses of all three ROMS simulations, especially GFDL-ROMS, differ from the findings
424 of Saba et al. (2016) who found that the warming in the Gulf of Maine at depth was due to a
425 northward shift of the Gulf Stream. There are several potential explanations for why the Gulf
426 of Maine warms without a northward shift in the Gulf Stream, as discussed in the section 4.
427 Given that wind stress (and thus zonally-integrated wind stress curl) is very different in the
428 three GCMs over the Atlantic Ocean (Fig. SM12), while the response of the currents is similar,
429 suggests that it is buoyancy forcing and changes in AMOC, rather than wind-driven changes
430 in the gyre circulation, that are critical for the Gulf Stream weakening in both the GCM and
431 ROMS simulations.
432
433 *f. Eddies*

Eddy activity is represented by the eddy kinetic energy (EKE, $0.5(u'^2 + v'^2)$), calculated from the currents in the surface layer, where the departures ($'$) are obtained from pentad values after subtracting a 120-day mean centered on that pentad. In the CTRL, eddies are prominent in the Gulf Stream after it separates from the coast, in the Loop Current region of the Gulf of Mexico, and southeast of the Yucatan Peninsula in summer (contours in Fig. 15). The general pattern of the change in eddies in all three simulations is similar to those of the currents, with a decrease in eddy activity in the center of the Gulf Stream region, where the maximum EKE occurs in the CTRL. In GFDL-ROMS there is a decrease in EKE on the northern flank of the Gulf Stream and a slight decrease on its southern edge, and these changes are slightly larger in JJA then in DJF. In contrast, in IPSL-ROMS and HadGEM-ROMS there is an increase (decrease) in EKE on the northern (southern) edge of the Gulf Stream in both DJF and JJA. This increase in EKE occurs in a narrow band from the coast northeastward for ~8º of longitude, but then becomes broader but more diffuse south of Nova Scotia (~65ºW) and further to the east. All three downscalled simulations show a decrease in eddy activity in the vicinity of the Loop Current in DJF, with an increase (decrease) on its western (eastern) side during JJA, but with enhanced EKE in the western half of the Gulf of Mexico (west of 90ºW) in winter as well as summer. Further south, the EKE differs between the simulations in the Caribbean Sea, where it generally decreases in the GFDL-ROMS in winter and on the western side of the sea in summer, but increases in the IPSL-ROMS and HadGEM-ROMS in both seasons.

4. Summary and Conclusions

456 We used the regional ocean model system (ROMS) with 7 km resolution to downscale the
457 effects of climate change on the western North Atlantic and Gulf of Mexico. First, a control
458 simulation (CTRL) was conducted using observationally-based atmosphere and ocean fields
459 as boundary conditions. Then monthly mean differences (Δs) in surface fluxes and ocean
460 conditions between 1976-2005 and 2070-2099 were obtained from three CMIP5 GCMs:
461 GFDL, IPSL, and HadGEM, and added to the CTRL. Finally, the response to anthropogenic
462 forcing was obtained from the difference between each of the three Δ-forced simulations and
463 the CTRL.
464 The climate change response in the three downscaled simulations, termed GFDL-ROMS,
465 IPSL-ROMS and HadGEM-ROMS, during winter (DJF) and summer (JJA) reflects both the
466 large-scale forcing and more regional changes resulting from mesoscale dynamics and
467 interaction with coastal features. All three simulations show strong increases in SSTs over most
468 of the domain, except in the vicinity of the US mid-Atlantic coast during DJF, where weaker
469 warming is associated with a reduction in strength of the Gulf Stream. Consistent with previous
470 studies, the weakening of the Gulf Stream is likely caused by a reduction in high latitude
471 buoyancy and a slowing of AMOC, as opposed to wind-driven changes in the gyre circulations,
472 since the wind stress changes across the Atlantic are very different in the three GCMs used to
473 drive ROMS. The difference in the SST response between the Gulf Stream and the surrounding
474 ocean decreases in summer as a shallow mixed layer forms and the heating from the
475 atmosphere is distributed over a thinner layer.
476 The large-scale forcing, however, can also result in substantial differences among the three
477 ROMS simulations. The warming of SSTs north of the Gulf Stream increases in magnitude
478 and extent from GFDL-ROMS to IPSL-ROMS to HadGEM-ROMS, with the response in

HadGEM-ROMS being approximately 1°-2.5°C stronger than in GFDL north of ~40°N. While the warming in HadGEM-ROMS tends to be largest at or near the surface, the maximum warming is often at depth in GFDL-ROMS.

The large-scale differences in the temperature and salinity response as a function of depth strongly influences the changes in nearshore regions, which are well resolved in the ROMS simulations but not in the GCMs. For example, the strongest warming in GFDL-ROMS enters the gulfs of Saint Lawrence and Maine near the bottom of deep channels, while the maximum warming occurs higher in the water column in the other two simulations resulting in greater warming along the banks of these two gulfs. The vertical structure of the salinity response is also markedly different in the three downscaled simulations in some regions. For example, the salinity decreases in the surface layer in the Gulf of Maine and increases at depth in GFDL-ROMS simulation, while the salinity increase extends over the depth of the Gulf in the other two simulations.

Differences in the downscalled simulations also arise in the Gulf of Mexico, where the largest increase in temperature occurs within the thermocline during winter in GFDL-ROMS and to a lesser degree in IPSL-ROMS, but occurs near the surface in HadGEM-ROMS. As a result, the stratification, as given by the difference in density between the surface and 100 m, actually decreases over the most of the Gulf of Mexico in GFDL-ROMS and IPSL-ROMS in winter, opposite to the general increase in stratification that is projected to occur over most of the world's oceans. The response is especially strong where thermocline abuts the shelf, creating exceptionally warm (> 4°C) bottom temperatures on the West Florida slope and shelf. Other processes also influence the response in the Gulf of Mexico. For example, changes in runoff from the Mississippi River, which greatly increases in HadGEM-ROMS, results in a

502 decrease in salinity in the northern Gulf. In addition, enhanced eddy activity occurs on the
503 western side of the Loop Current and extends across the western portion of the basin in all
504 three downscaled simulations, suggesting that more eddies may shed from the Loop Current
505 and propagate westward in the future. Thus, a wide array of both atmosphere and ocean
506 processes may influence how climate change unfolds in the Gulf of Mexico.

507 In addition to the overall reduction in the strength of the western boundary current system,
508 including the Yucatan, Loop and Florida currents as well as the Gulf Stream, the fine resolution
509 in the ROMS simulations allows for regional ocean circulation changes. The Gulf Stream
510 exhibits a southward shift in GFDL-ROMS and a slight northward shift in the other two ROMS
511 simulations. The northward shift is part of an elongated anticyclonic gyre circulation which
512 reaches approximately 72ºW and 65ºW in the IPSL-ROMS and HadGEM-ROMS,
513 respectively. A commensurate meridional shift occurs in the eddy kinetic energy. However, all
514 three model simulations suggest that the changes in the Gulf Stream remain well to the south
515 of New England and that climate change enhances the present-day circulation, with water
516 entering the Gulf of Maine from the east and then flowing counterclockwise around the basin.
517 In addition, back trajectories based on the GFDL-driven ROMS circulation changes indicate
518 that the water arriving in the Gulf Maine via the northeast channel mainly originated from the
519 central North Atlantic (Sang-Ik Shin, personal communication). In contrast, using a high-
520 resolution global model, Saba et al. (2016) found that enhanced warming at depth in the Gulf
521 of Maine was due to a northward shift of the Gulf Stream.

522 Since the northward shift of the Gulf Stream does not appear to directly cause the enhanced
523 warming in the northeast portion of the ROMS domain, what processes could be involved in

524 the very strong response in the gulfs of Maine and Saint Lawrence? The enhanced warming
525 may result from a number of processes including:

526 • Very strong warming of the atmosphere over eastern Canada (> 8°C) that is transported
527 over the Atlantic due to advection by westerly winds (see Fig. 3), heating the ocean via
528 changes in the surface fluxes. This atmospheric related heating may partly explain the
529 warming adjacent to the northeast US and Atlantic Canadian provinces as indicated by
530 present day ocean heat budget analyses (Chen et al. 2015, 2016) and by climate
531 equilibrium studies in which greenhouse gasses are increased (often doubled) in a
532 global atmospheric model that is coupled to an ocean model without currents (e.g.
533 Danabasoglu and Gent 2009; Dommenget 2012). The increase in surface air
534 temperatures over North America is modest, intermediate, and strong in the GFDL,
535 IPSL and HadGEM models respectively, which corresponds to the magnitude of the
536 warming of SSTs off the coast of New England and Canada's Atlantic provinces in
537 both the GCMs and the corresponding ROMS simulations.

538 • With polar amplification of the climate change signal, the Arctic Ocean and Labrador
539 Sea are projected to undergo very strong warming by the end of the 21st century,
540 especially in regions where the ice has retreated from. This much warmer water relative
541 to today's climate can then be advected by the east Greenland current and Labrador
542 currents from Newfoundland to the northeast US coast.

543 • The reduction in AMOC enhances the absorption of heat from the atmosphere at high
544 latitudes (Rugenstein et al. 2013), which can subsequently be advected by the Labrador
545 current to the NE US Shelf as described above.

- CMIP5 models, including the three used here, indicate a small region of very strong warming in the vicinity of ~44°N-45°W, southeast of Newfoundland, associated with more northward directed currents in the future (Fig SM13). While most of the changes in currents are directed towards the southwest, these changes in temperature and currents appear to be linked to the overall reduction in AMOC (Cheng et al. 2013, Winton et al. 2013). The very warm water can subsequently be advected towards the coast.
- Ocean eddies in the vicinity of the Gulf Stream may transport warm salty water towards the NE US shelf, especially in the IPSL-ROMS and HadGEM- ROMS simulations, where there are semi-permanent eddies south of Nova Scotia (Fig. 12) and an increase in transient eddy activity on the northern flank of the Gulf Stream/North Atlantic Current (Fig 14).

The differences between the three ROMS simulations, and between the ROMS simulations and the high-resolution global model simulation analyzed by Saba et al. 2016, indicate that while high resolution allows for better representation of the large-scale and regional circulation, it doesn't guarantee the same climate change response, which depends on a wide range of factors. These findings suggest that even when using dynamically downscaled regional ocean models or high-resolution global models to investigate the oceanic response to climate change, one should use ensembles of global models to capture structural uncertainty in the models and the range of potential outcomes that result.

Acknowledgements

We thank Michael Jacox and the reviewers for their constructive comments. This study is supported by a grant from the NOAA Coastal and Climate Applications (COCA) program #NA-15OAR4310133.

References

Alexander MA, JD Scott, KD Friedland, KE Mills, JA Nye, AJ Pershing, AC Thomas, 2018: Projected sea surface temperatures over the 21st century: Changes in the mean, variability and extremes for large marine ecosystem regions of Northern Oceans. *Elementa: Science of the Anthropocene*, **6(1):9**, DOI: http://doi.org/10.1525/elementa.191

Auad, G, Miller A, Di Lorenzo E. 2006. Long-term forecast of oceanic conditions off California and their biological implications. J. Geophys. Res.-Oceans. 111 10.1029/2005jc003219 .

Belkin, IM 2009 Rapid warming of Large Marine Ecosystems. Prog Oceanogr. 81(1–4): 207–213. DOI: https:// doi.org/10.1016/j.pocean.2009.04.011

Boyer, T.P.; Levitus, S.; Antonov, J.I.; Locarnini, R.A.; Garcia, H.E., 2005: Linear trends in salinity for the World Ocean, 1955–1998. Geophys. Res. Lett. 32, doi:10.1029/2004GL021791.

590 Bryan, F. O., M. W. Hecht, and R. D. Smith, 2007: Resolution convergence and sensitivity
591 studies with North Atlantic circulation models. Part I: The western boundary current
592 system, Ocean Modell., 16, 141–159, doi:10.1016/j.ocemod.2006.08.005.
593
594 Capotondi, A., M. A. Alexander, N. A. Bond, E. N. Curchitser, and J. D. Scott, 2012: Enhanced
595 upper ocean stratification with climate change in the CMIP3 models, *J. Geophys. Res.*, **117**,
596 C04031, doi:10.1029/2011JC007409.
597
598 Carton, J. A., and B. S. Giese, 2008: A reanalysis of ocean climate using Simple Ocean Data
599 Assimilation (SODA). *Mon. Wea. Rev.*, **136**, 2999–3017,
600 doi:https://doi.org/10.1175/2007MWR1978.1.
601
602 Caesar, L., S. Rahmstorf, A. Robinson, G. Feulner, and Saba, V, 2018: Observed fingerprint
603 of a weakening Atlantic Ocean overturning circulation. *Nature Climate Change*, **556**, 191-
604 196, doi: 10.1038/s41586-018-0006-5.
605
606 Chen K., G. G. Gawarkiewicz, S. J. Lentz S. J., and Bane, 2014: Diagnosing the warming of
607 the Northeastern US Coastal Ocean in 2012: A linkage between the atmospheric jet stream
608 variability and ocean response. Journal of Geophysical Research: Oceans, 119, 218–227.
609
610 Chen, K., G. Gawarkiewicz, Y.-O. Kwon, and W. G. Zhang, 2015: Role of atmospheric forcing
611 versus ocean advection during the anomalous warming on the Northeast U.S. shelf in
612 2012, *J. Geophys. Res.*, **120**, 4324–4339, doi:10.1002/2014JC010547.

Chen, K., Y.-O. Kwon, and G. Gawarkiewicz, 2016: Interannual Variability of Winter-Spring Temperature in the Middle Atlantic Bight: Relative Contributions of Atmospheric and Oceanic Processes. *J. Geophys. Res.*, **121**, 4209–4227. 10.1002/2016JC011646.

Cheng, W., J.C. Chiang, and D. Zhang, 2013: Atlantic Meridional Overturning Circulation (AMOC) in CMIP5 Models: RCP and Historical Simulations. *J. Climate,* **26**, 7187–7197, https://doi.org/10.1175/JCLI-D-12-00496.1

Collins, M., R. Knutti, J. Arblaster, J.-L. Dufresne, T. Fichefet, P. Friedlingstein, X. Gao, W.J. Gutowski, T. Johns, G. Krinner, M. Shongwe, C. Tebaldi, A.J. Weaver and M. Wehner, 2013: Long-term Climate Change: Projections, Commitments and Irreversibility. In: Climate Change 2013: The Physical Science Basis. Contribution of Working Group I to the Fifth Assessment Report of the Intergovernmental Panel on Climate Change [Stocker, T.F., D. Qin, G.-K. Plattner, M. Tignor, S.K. Allen, J. Boschung, A. Nauels, Y. Xia, V. Bex and P.M. Midgley (eds.)]. Cambridge University Press, Cambridge, United Kingdom and New York, NY, USA.

Coumou, D., G. Di Capua, S. Vavrus, L. Wang, S. Wang, 2018: The influence of Arctic amplification on mid-latitude summer circulation. *Nature Communications*, **9**, Article number: 2959. 10.1038/s41467-018-05256-8

635 Dai., A., T. Qian, K. E. Trenberth and J. D. Milliman, 2009: Changes in continental freshwater
636 discharge from 1948-2004, J. Climate, 22, 2773-2792.
637
638 Danabasoglu, G., 2008: On Multidecadal Variability of the Atlantic Meridional Overturning
639 Circulation in the Community Climate System Model Version 3. *J. Climate,* **21**,5524–
640 5544, https://doi.org/10.1175/2008JCLI2019.1
641
642 Danabasoglu, G. and P.R. Gent, 2009: Equilibrium Climate Sensitivity: Is It Accurate to Use
643 a Slab Ocean Model?. *J. Climate,* **22**, 2494–2499,
644 https://doi.org/10.1175/2008JCLI2596.1
645
646 Dommenget, D., 2012: Comments on "The Relationship between Land–Ocean Surface
647 Temperature Contrast and Radiative Forcing", *J. Climate*, **25**, 3437–3440.
648
649 Drijfhout, S., van Oldenborgh, G. J. and Cimatoribus, A., 2012: Is a decline of AMOC causing
650 the warming hole above the North Atlantic in observed and modeled warming patterns? *J.*
651 *Clim.*, 25, 8373–8379 (2012).
652
653 Flato, G., J. Marotzke, B. Abiodun, P. Braconnot, S.C. Chou, W. Collins, P. Cox, F. Driouech,
654 S. Emori, V. Eyring, C. Forest, P. Gleckler, E. Guilyardi, C. Jakob, V. Kattsov, C. Reason
655 and M. Rummukainen, 2013: Evaluation of Climate Models. In: *Climate Change 2013:*
656 *The Physical Science Basis. Contribution of Working Group I to the Fifth Assessment*
657 *Report of the Intergovernmental Panel on Climate Change* [Stocker, T.F., D. Qin, G.-K.

Plattner, M. Tignor, S.K. Allen, J. Boschung, A. Nauels, Y. Xia, V. Bex and P.M. Midgley (eds.)]. Cambridge University Press, Cambridge, United Kingdom and New York, NY, USA.

Gregory, J. M., et al. (2005), A model intercomparison of changes in the Atlantic thermohaline circulation in response to increasing atmospheric CO2 concentration, *Geophys. Res. Lett.*, **32**, L12703, doi:10.1029/ 2005GL023209.

Hare, J. A., J. Manderson, J. Nye, M. Alexander, P. J. Auster, D. Borggaard, A. Capotondi, K. Damon-Randall, E. Heupel, I. Mateo, L. O'Brien, D. Richardson, C. Stock, and S. T. Biegel, 2012: Cusk (Brosme brosme) and climate change: assessing the threat to a candidate marine fish species under the U.S. Endangered Species Act *ICES Journal of Marine Science*, **69**, 1753-1768.

Hermann, A. J., G. A. Gibson, N. A. Bond, E. N. Curchitser, K. Hedstrom, W. Cheng, M. Wang, E. D. Cokelet, P. J. Stabeno and K. Aydin. 2016. Projected future biophysical states of the Bering Sea. *Deep-Sea Res. II*, **134**, 30-47, http://dx.doi.org/10.1016/j.dsr2.2015.11.001.

Heuzé, C., 2017: North Atlantic deep water formation and AMOC in CMIP5 models. Ocean Science. 13. 609-622. 10.5194/os-13-609-2017.

680 Kang, D., and E. N. Curchitser, 2013: Gulf Stream eddy characteristics in a high-resolution
681 ocean model. *J. Geophys. Res. Oceans*, **118**, 4474–4487,
682 doi:https://doi.org/10.1002/jgrc.20318.
683
684 Kang, D. and E.N. Curchitser, 2015: Energetics of Eddy–Mean Flow Interactions in the Gulf
685 Stream Region. *J. Phys. Oceanogr.,* **45**, 1103–1120,https://doi.org/10.1175/JPO-D-14-
686 0200.1
687
688 Karspeck, A.R., Stammer, D., Köhl, A. et al., 2017: Comparison of the Atlantic meridional
689 overturning circulation between 1960 and 2007 in six ocean reanalysis products. *Clim.*
690 *Dyn.* **49:** 957. https://doi.org/10.1007/s00382-015-2787-7.
691
692 Knutson, TR, Zeng, F and Wittenberg, AT 2013 Multimodel assessment of regional surface
693 temperature trends: CMIP3 and CMIP5 twentieth-century Simulations. *J. Climate,*
694 **26**(22): 8709–8743. DOI: https://doi.org/10.1175/JCLI-D-12-00567.1 K
695

Large, W. G., and S. G. Yeager, 2009: The global climatology of an interannually varying air–sea flux data set. *Climate Dyn.*, **33**, 341–364, doi:https://doi.org/10.1007/s00382-008-0441-3.

696 Lima, F. P. and Wethey, D. S., 2012: Three decades of high-resolution coastal sea surface
697 temperatures reveal more than warming. *Nat. Commun.* 3:704 doi: 10.1038/ncomms1713.
698

699 Liu, Y., S.-K. Lee, B. A. Muhling, J. T. Lamkin, and D. B. Enfield, 2012: Significant reduction
700 of the Loop Current in the 21st century and its impact on the Gulf of Mexico, *J. Geophys.*
701 *Res.*, 117, C05039, doi:10.1029/2011JC007555.
702
703 Liu Y., S.-K. Lee, D. B. Enfield, B. A. Muhling, J. T. Lamkin, F. E. Muller-Karger, M. A.
704 Roffer, 2015: Potential impact of climate change on the Intra-Americas Sea: Part-1. A
705 dynamic downscaling of the CMIP5 model projections. J. Mar. Sys., 148, 56-69, ISSN
706 0924-7963, https://doi.org/10.1016/j.jmarsys.2015.01.007.
707
708 Liu, Z.-J., S. Minobe, Y. N. Sasaki, and M. Terada, 2016: Dynamical downscaling of future
709 sea level change in the western North Pacific using ROMS. *J. of Oceanogr.,* **72**.
710 10.1007/s10872-016-0390-0.
711
712 Pauly, D., and D. Zeller, editors (2016) *Global atlas of marine fisheries: A critical appraisal*
713 *of catches and ecosystem impacts*. Washington, DC: Island Press, 486 p.
714
715 Pedersen, R.A., I. Cvijanovic, P.L. Langen, and B.M. Vinther, 2016: The Impact of Regional
716 Arctic Sea Ice Loss on Atmospheric Circulation and the NAO. *J. Climate,* **29**,889–
717 902, https://doi.org/10.1175/JCLI-D-15-0315.1
718
719 Pershing, A. J., M. A. Alexander, C. M. Hernandez, L. A. Kerr, A. Le Bris, K. E. Mills, J. A.
720 Nye, N. R. Record, H. A. Scannell, J. D. Scott, G. D. Sherwood, and A. C. Thomas, 2015:

Slow Adaptation in the Face of Rapid Warming Leads to the Collapse of Atlantic Cod in the Gulf of Maine. *Science*, 10.1126/science.aac9819.

Rugenstein, M.A., M. Winton, R.J. Stouffer, S.M. Griffies, and R. Hallberg, 2013: Northern High-Latitude Heat Budget Decomposition and Transient Warming. *J. Climate,* **26**,609–621, https://doi.org/10.1175/JCLI-D-11-00695.1

Saba, V. S., S. M. Griffes, W. G. Anderson, M. Winton, M. A. Alexander, T. L. Delworth, J. A. Hare, M. J. Harrison, A. Rosati, G. A. Vechhi, R. Zhang, 2016: Enhanced warming of the Northwest Atlantic Ocean under climate change. *J. Geophys. Res.: Oceans*, **121**, 118-132, doi:10.1002/2015JC011346.

Shchepetkin, A. F., and J. C. McWilliams, 2003: A method for computing horizontal pressure-gradient force in an oceanic model with a nonaligned vertical coordinate, *J. Geophys. Res.*, **108**(C3), 3090, doi:10.1029/2001JC001047.

Shchepetkin, A. F., and J. C. McWilliams, 2005: The Regional Oceanic Modeling System (ROMS): A split-explicit, free-surface, topography-following-coordinate oceanic model, *Ocean Modell.*, **9**, 347–404.

Shearman, R.K. and S.J. Lentz, 2010: Long-Term Sea Surface Temperature Variability along the U.S. East Coast. *J. Phys. Oceanogr.,* **40**, 1004–1017,https://doi.org/10.1175/2009JPO4300.1

Sun, L., M. Alexander, and C. Deser, 2018: Evolution of the Global Coupled Climate Response to Arctic Sea Ice Loss during 1990-2090 and Its Contribution to Climate Change. *J. Climate*, **31**, 7823-7843, https://doi.org/10.1175/JCLI-D-18-0134.1

van Hooidonk, R.V., J. A. Maynard, Y. Liu, S.-K. Lee, 2015: Downscaled projections of Caribbean coral bleaching that can inform conservation planning. *Global Change Biology*, **21**, 3389–3401, doi: 10.1111/gcb.12901.

Winton, M., S.M. Griffies, B.L. Samuels, J.L. Sarmiento, and T.L. Frölicher, 2013: Connecting Changing Ocean Circulation with Changing Climate. *J. Climate,* **26**, 2268–2278, https://doi.org/10.1175/JCLI-D-12-00296.1

Winton, M., W. G. Anderson, T. L. Delworth, S. M. Griffies, W. J. Hurlin, and A. Rosati, 2014: Has coarse ocean resolution biased simulations of transient climate sensitivity?, Geophys. Res. Lett., 41, 8522–8529, doi:10.1002/ 2014GL061523.

Wu, L., W. Cai, L. Zhang, H. Nakamura, A. Timmermann, T. Joyce, M. J. McPhaden, M. Alexander, B. Qiu, M. Visbeck, P. Chang, and B. Giese, 2012: Enhanced warming over the global subtropical western boundary currents. *Nature Climate Change*. DOI: 10.1038/NCLIMATE1353.

766 Xiu, P., F. Chai, E. N. Curchitser, and F. S. Castruccio, 2018: Future changes in coastal
767 upwelling ecosystems with global warming: The case of the California Current System.
768 *Scientific Reports*, **8**, article number 2866, 10.1038/s41598-018-21247-7.
769
770
771

772 Table 1. The three global climate models (GCMs) used to compute the delta (Δ) values, the
773 mean difference between the periods (2070-2099) and (1976-2005), to incorporate the large-
774 scale climate change forcing. The transient climate response, the change in global and annual
775 mean surface temperature from an experiment in which the CO_2 concentration is increased by
776 1% yr^{-1}, and calculated using the difference between the start of the experiment and a 20-year
777 period centered on the time of CO_2 doubling (Flato et al. 2013). The AMOC values (in Sv)
778 are given by the maximum overturning stream function value in the Atlantic and their (see).
779 The TCR and AMOC are indicated as weak, moderate and strong relative to the large set of
780 CMIP5 models (Flato et al. 2013; Cheng et al. 2013; Collins et al. 2013; Heuzé 2017).
781

Modeling Center	**Model**	**Atmosphere Resolution**	**Ocean Resolution**	**Transient Climate Response**	**AMOC Strength 1976-2005**	**ΔAMOC Strength**
NOAA Geophysical Fluid Dynamics Laboratory (GFDL) USA	ESM2M	2° lat x 2.5° lon; 24 levels	~1° lat x 1° lon; Meridional resolution increases from 30° N/S to 1/3° on the equator; tripolar grid > 65°N; 50 levels	1.3 Weak	17.9 Sv Moderate	-6.9 Sv strong
Institut Pierre-Simon Laplace (IPSL) France	CM5A-MR	1.25° lat x 2.5° lon; 39 levels	~2° lat x 2° lon; meridional resolution increases to ½° on the equator; 31 levels	2.0 Moderate	12.2 Weak	-3.9 Weak
Met Office Hadley Center (Had) UK	HadGEM2-CC	1.875° lat × 1.25° lon; 38 levels	~1° lat x 1° lon Increases from 30° N/S to 1/3° on the equator; 40 levels	2.5 Strong	16.8 Moderate	-4.4 Weak-to-Moderate

782

Figure Captions

Fig. 1. ROMS domain with (a) bathymetry (shaded, 25 m interval) at 1.85 km resolution. White lines/transects depict the locations of cross-sections shown in Figs. 7, 8, 9, 12, 14. (b) Annual mean surface currents (shaded, interval 10 cm s^{-1}) from the ROMS control (CTRL) experiment.

Fig. 2. SST in the CTRL (contours, interval 2 ˚C) and the SST response to climate change (RCP8.5 – CTRL, shaded, interval 0.5 ˚C) during DJF (top row) and JJA (bottom row) in ROMS driven by three GCMs: (a) (d) GFDL-ROMS, (b) (e) IPSL-ROMS, and (c) (f) HadGEM-ROMS. The surface and boundary conditions for the CTRL are obtained from reanalysis during 1976-2005 (historical period), with additional forcing added to the CTRL that is derived from the mean difference between 2070-2099 and 1976-2005 in the three RCP8.5 experiments.

Fig. 3. Surface air temperature change (RCP8.5 – historical period, shaded 1.0 ˚C interval) and the surface winds in the RCP8.5 simulations from 2070-2099 (vectors, scale bottom right) during DJF (top) and JJA (bottom) in the (a) (d) GFDL (b) (e) IPSL, and (c) (f) HadGEM GCMs. Highlights how enhanced warming over North America, especially over Canada in winter, could be advected by the winds warming the coastal ocean in the future.

Fig. 4. Bottom temperature response (RCP8.5 – CTRL, shaded, interval 0.5 ˚C) during DJF (top row) and JJA (bottom row) in (a) (d) GFDL-ROMS, (b) (e) IPSL-ROMS, and (c) (f) HadGEM-ROMS. The 200m isobath, representing the shelf break, is indicated by the black curve.

Fig. 5. Sea surface salinity (SSS) response (RCP8.5 – CTRL, shaded, interval 0.1 PSU) during DJF (top row) and JJA (bottom row) in (a) (d) GFDL-ROMS, (b) (e) IPSL-ROMS, and (c) (f) HadGEM -ROMS.

Fig. 6. Bottom salinity response (RCP8.5 – CTRL, shaded, interval 0.1 PSU) during DJF (top row) and JJA (bottom row) in (a) (d) GFDL-ROMS, (b) (e) IPSL-ROMS, and (c) (f) HadGEM-ROMS. The 200m isobath is indicated by the black curve.

Fig. 7. Cross section of the annual mean temperature (top) and salinity (bottom) along the Laurentian Channel in ROMS. Shown are the temperature from CTRL (contour, interval 1.0 ˚C) and the response (shaded, interval 0.5 ˚C) and salinity from the CTRL (contour, interval 0.5 PSU) and the response (shaded, interval 0.1 PSU) in (a) (d) GFDL-ROMS, (b) (e) IPSL-ROMS, and (c) (f) HadGEM -ROMS. Note the section is along the bottom of channel (not a straight line) and extends from the southeast to northwest, from (A) to (B) in Fig. 1.

Fig. 8. Cross section of the annual mean temperature (top) and salinity (bottom) into the Gulf of Maine in ROMS. Shown are the temperature from CTRL (contour, interval 1.0 ˚C) and the response (shaded, interval 0.5 ˚C) and salinity from the CTRL (contour, interval 0.25 PSU) and the response (shaded, interval 0.05 PSU) in (a) (d) GFDL-ROMS, (b) (e) IPSL-ROMS, and (c) (f) HadGEM-ROMS. Note the section is in the deepest part of the Gulf (not a straight line) and extends from east to west, from (C) to (D) in Fig. 1.

Fig. 9. Cross section of the annual mean temperature (top) and salinity (bottom) along 28 ˚N in the Northern Gulf of Mexico in ROMS. Shown are the temperature from CTRL (contour, interval 1.0 ˚C) and the response (shaded, interval 0.5 ˚C) and salinity from the CTRL (contour, interval 0.5 PSU) and the response (shaded, interval 0.075 PSU) in (a) (d) GFDL-ROMS, (b) (e) IPSL-ROMS, and (c) (f) HadGEM-ROMS.

Fig. 10. Static stability, derived from the density difference between 100 m and the surface, in the CTRL (contours, interval 0.25 kg m^{-3}) and the static stability response (RCP8.5-CTRL, shaded, interval 0.025 kg m^{-3}) in ROMS during DJF (top row) and JJA (bottom row) in (a) (d) GFDL-ROMS, (b) (e) IPSL-ROMS, and (c) (f) HadGEM-ROMS.

Fig.11. Surface current response (RCP8.5 – CTRL, speed shown by shading, interval 5.0 cm s^{-1}) in ROMS during DJF (top row) and JJA (bottom row) in (a) (d) GFDL-ROMS, (b) (e) IPSL-ROMS, and (c) (f) HadGEM-ROMS.

Fig. 12. Cross section of the annual mean meridional velocity along 30˚N in the western North Atlantic in ROMS. Shown are the velocity from the CTRL (contours, interval 10 cm s^{-1}) and the response (RCP8.5 – CTRL, shading, interval 2.5 cm s^{-1}) in (a) (d) GFDL-ROMS, (b) (e) IPSL-ROMS, and (c) (f) HadGEM-ROMS.

Fig.13. Annual mean surface current off the northeast US coast in the (a) CTRL (2.5 cm s^{-1} shading interval), and the current response (RCP8.5 – CTRL, shaded, interval 0.25 cm s^{-1}) in (b) GFDL-ROMS, (c) IPSL-ROMS and (d) HadGEM-ROMS.

Fig. 14. Cross section of the annual mean meridional velocity along 70˚W in the western North Atlantic in ROMS. Shown are the velocity from the CTRL (contours, interval 5 cm s^{-1}) and the response (RCP8.5 – CTRL, shading, interval 2.5 cm s^{-1}) in (a) GFDL-ROMS, (b) IPSL-ROMS, and (c) HadGEM-ROMS.

Fig. 15. Surface eddy kinetic energy (EKE) in the CTRL (contours, interval 100 cm^2 s^{-2} starting at 500) and the EKE response (RCP8.5-CTRL, shaded, interval 25 cm^2 s^{-2}) in ROMS during DJF (top row) and JJA (bottom row) in(a) (d) GFDL-ROMS, (b) (e) IPSL-ROMS, and (c) (f) HadGEM-ROMS. The EKE is computed by removing 120-day running mean from the 5-day average velocity.

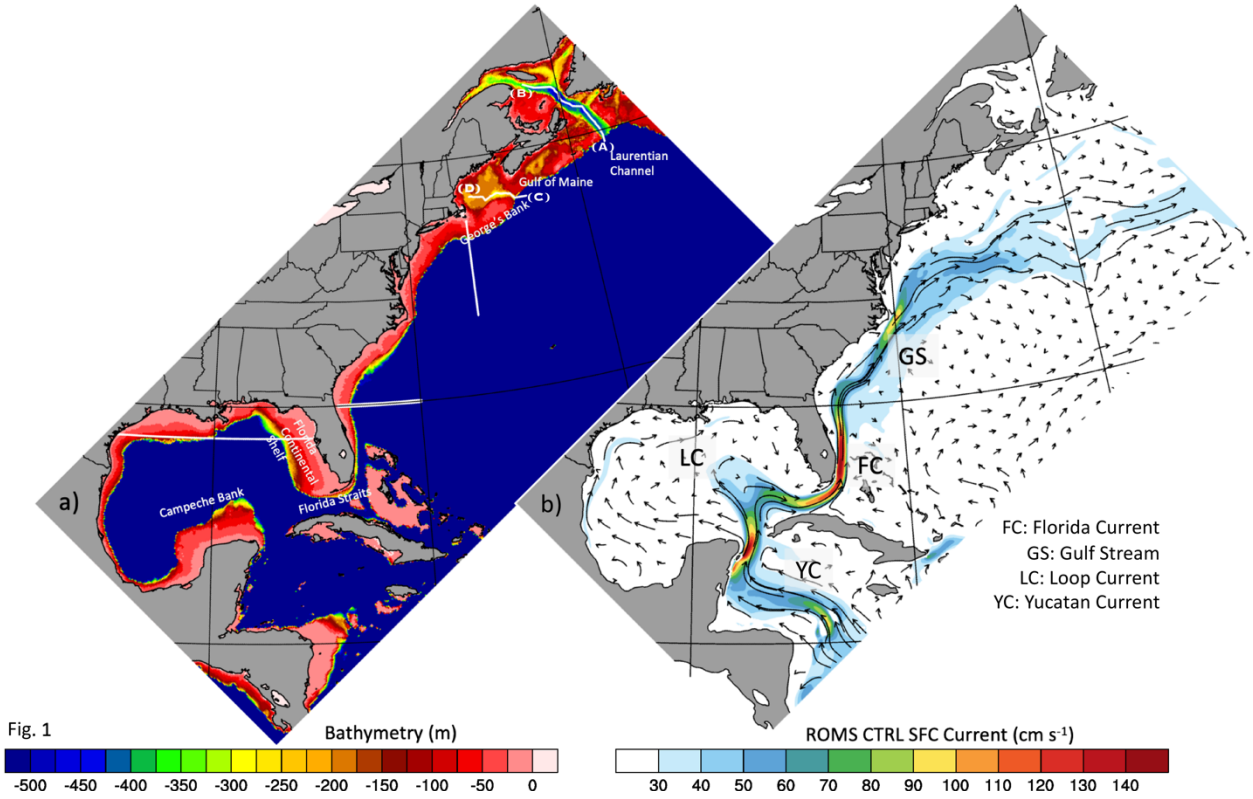

Fig. 1

Fig. 1. ROMS domain with (a) bathymetry (shaded, 25 m interval) at 1.85 km resolution. White lines/transects depict the locations of cross-sections shown in Figs. 7, 8, 9, 12, 14. (b) Annual mean surface currents (shaded, interval 10 cm s^{-1}) from the ROMS control (CTRL) experiment

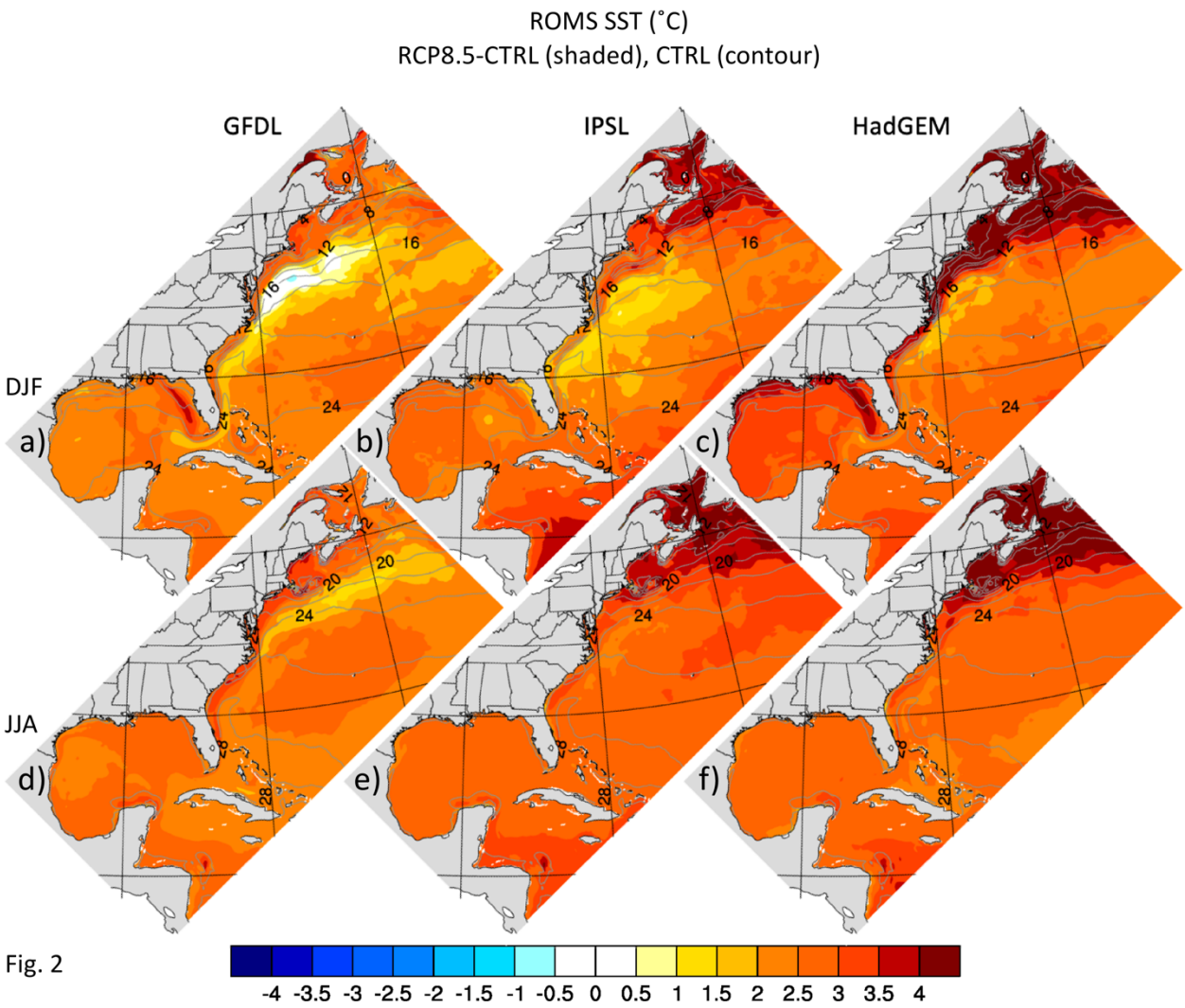

Fig. 2

Fig. 2. SST in the CTRL (contours, interval 2 ˚C) and the SST response to climate change (RCP8.5 – CTRL, shaded, interval 0.5 ˚C) during DJF (top row) and JJA (bottom row) in ROMS driven by three GCMs, i.e. (a) (d) GFDL-ROMS, (b) (e) IPSL-ROMS, and (c) (f) HadGEM-ROMS. The surface and boundary conditions for the CTRL are obtained from reanalysis during 1976-2005 (historical period), with additional forcing added to the CTRL that is derived from the mean difference between 2070-2099 and 1976-2005 in the three RCP8.5 experiments.

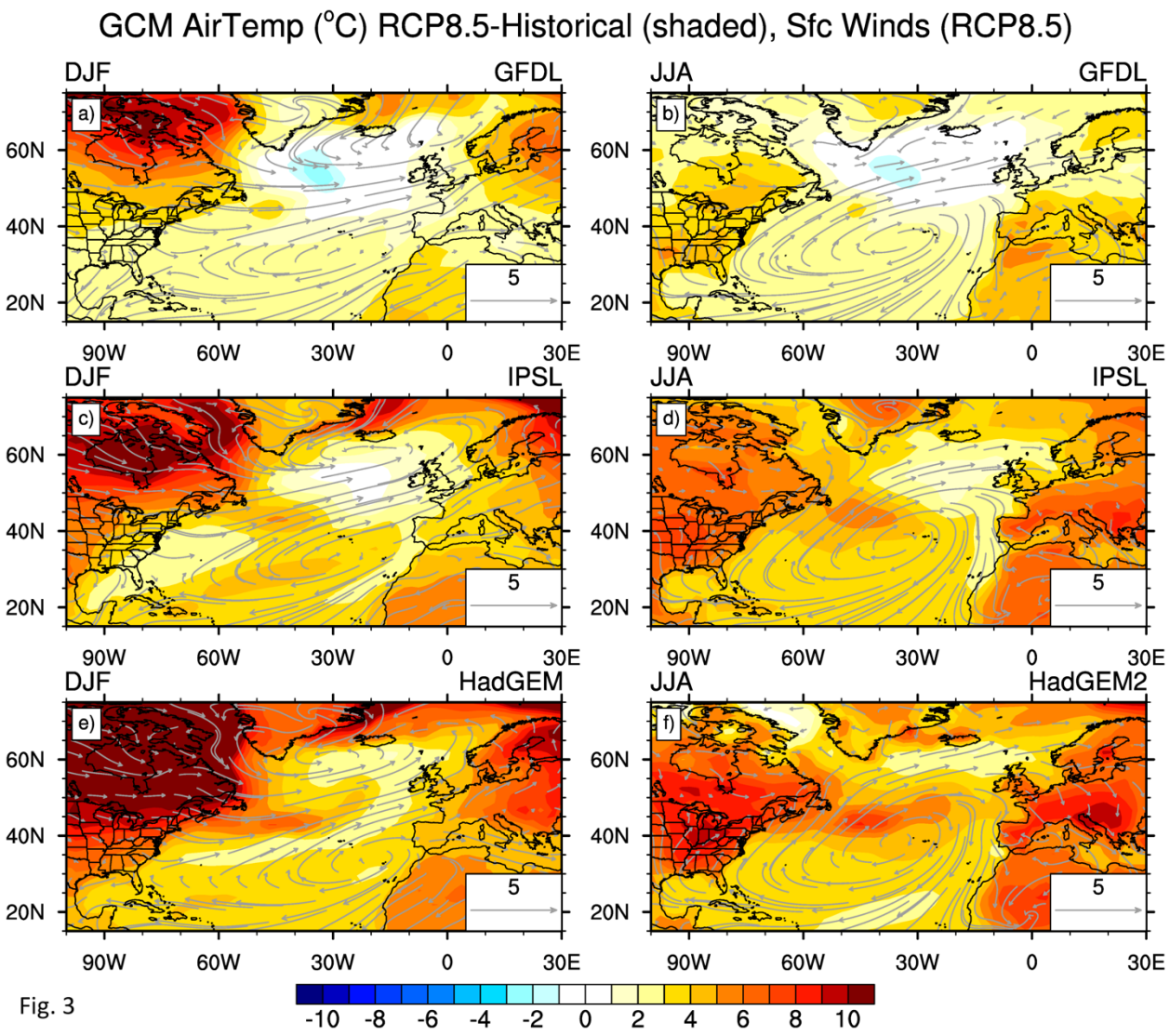

Fig. 3

Fig. 3. Surface air temperature change (RCP8.5 – historical period, shaded 1.0 ˚C interval) and the surface winds in the RCP8.5 simulations from 2070-2099 (vectors, scale bottom right) during DJF (top) and JJA (bottom) in the (a) (d) GFDL, (b) (e) IPSL, and (c) (f) HadGEM GCMs. Highlights how enhanced warming over North America, especially over Canada in winter, could be advected by the winds warming the coastal ocean in the future.

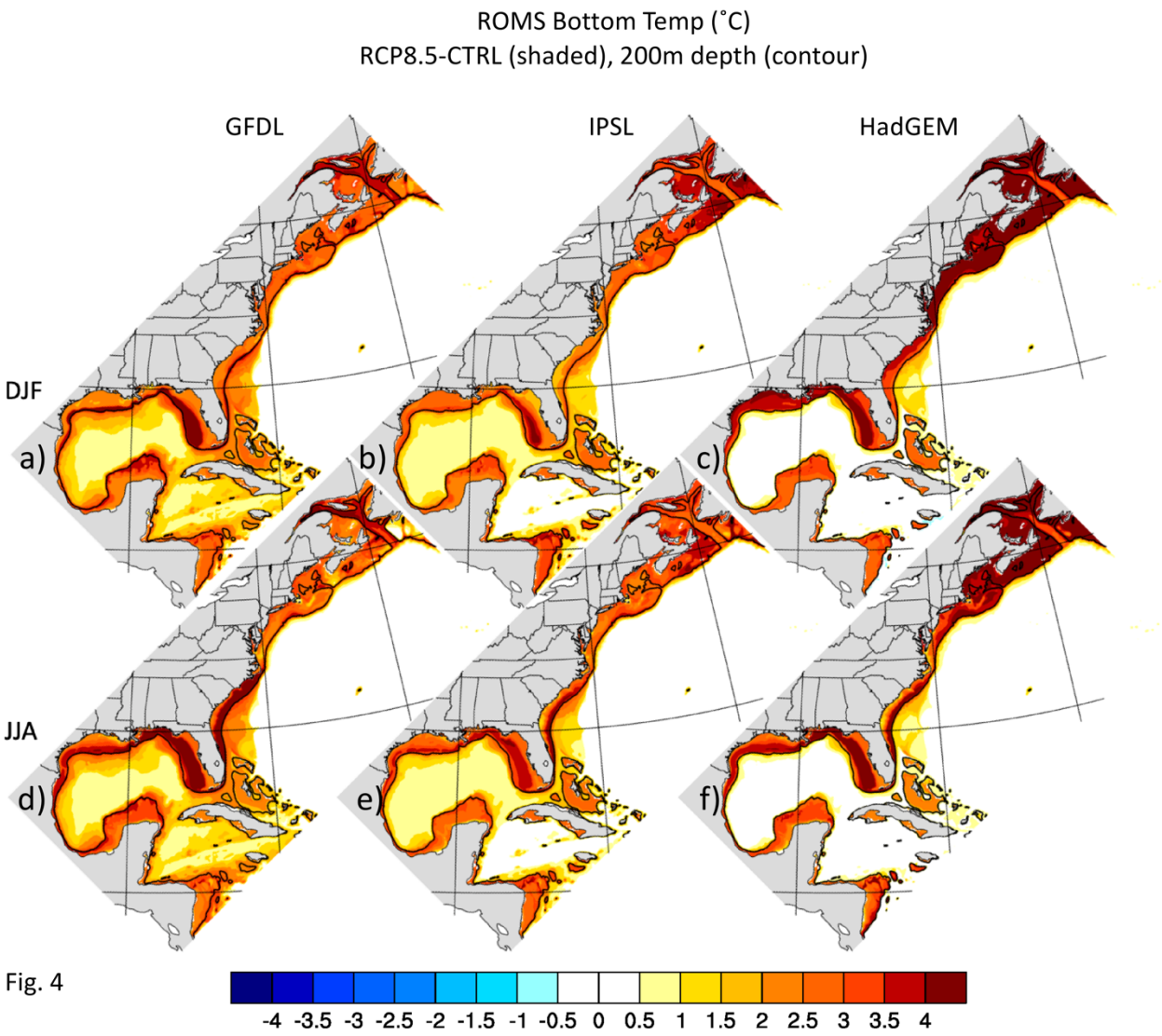

Fig. 4

Fig. 4. Bottom temperature response (RCP8.5 – CTRL, shaded, interval 0.5 ˚C) during DJF (top row) and JJA (bottom row) in (a) (d) GFDL-ROMS, (b) (e) IPSL-ROMS, and (c) (f) HadGEM-ROMS. The 200m isobath, representing the shelf break, is indicated by the black curve.

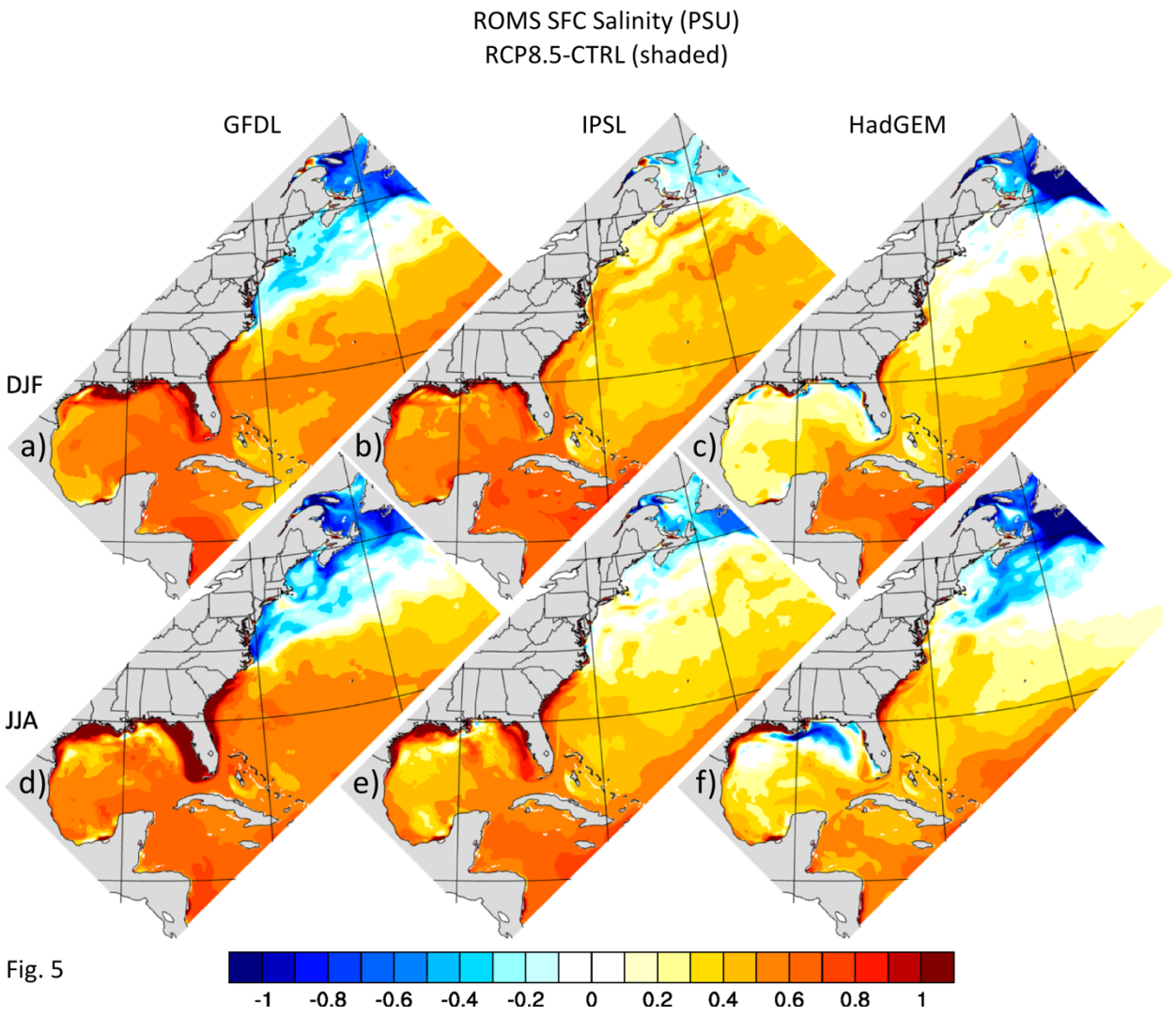

Fig. 5

Fig. 5. Sea surface salinity (SSS) response (RCP8.5 – CTRL, shaded, interval 0.1 PSU) during DJF (top row) and JJA (bottom row) in (a) (d) GFDL-ROMS, (b) (e) IPSL-ROMS, and (c) (f) HadGEM -ROMS.

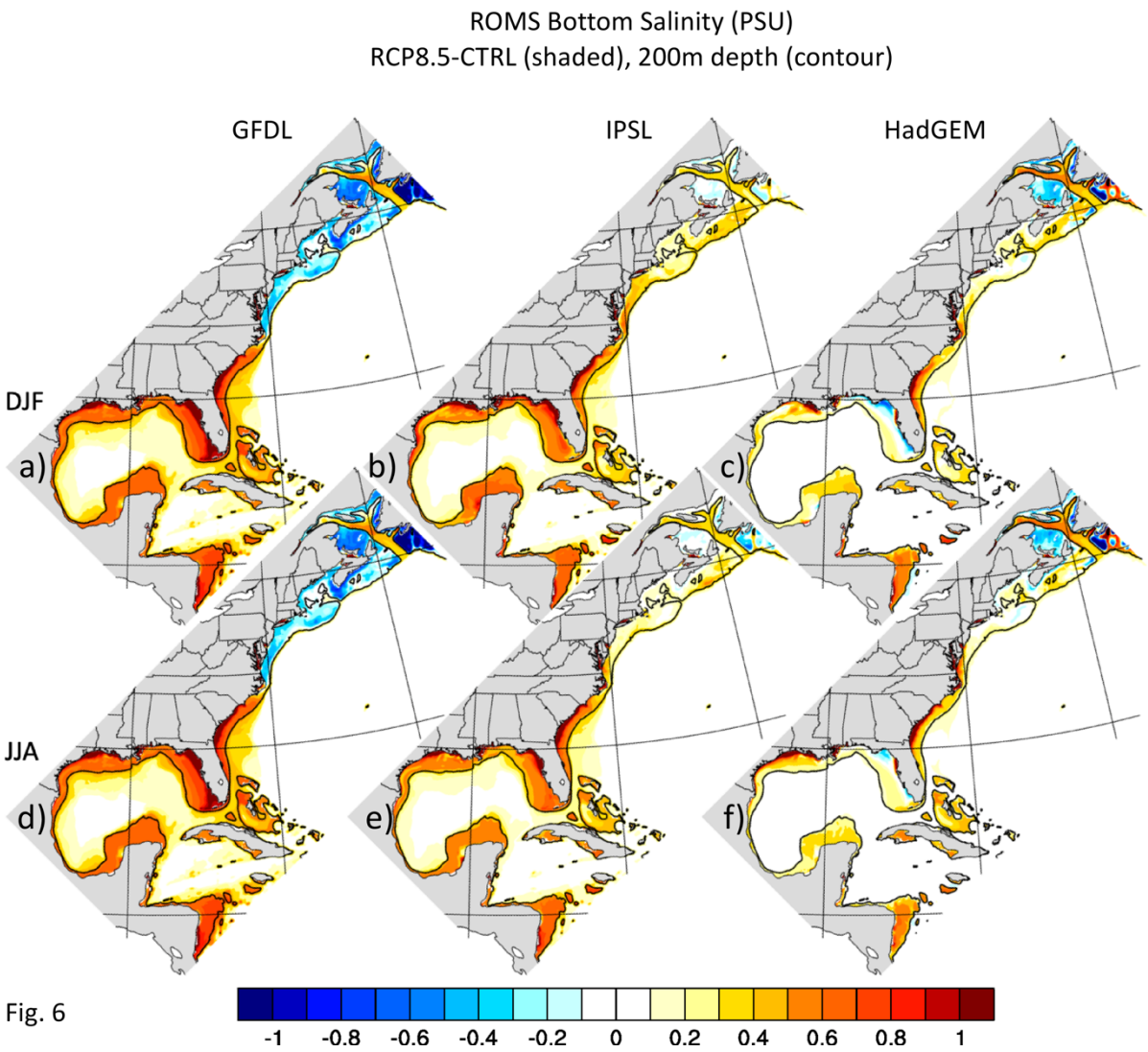

Fig. 6

Fig. 6. Bottom salinity response (RCP8.5 – CTRL, shaded, interval 0.1 PSU) during DJF (top row) and JJA (bottom row) in (a) (d) GFDL-ROMS, (b) (e) IPSL-ROMS, and (c) (f) HadGEM-ROMS. The 200m isobath is indicated by the black curve.

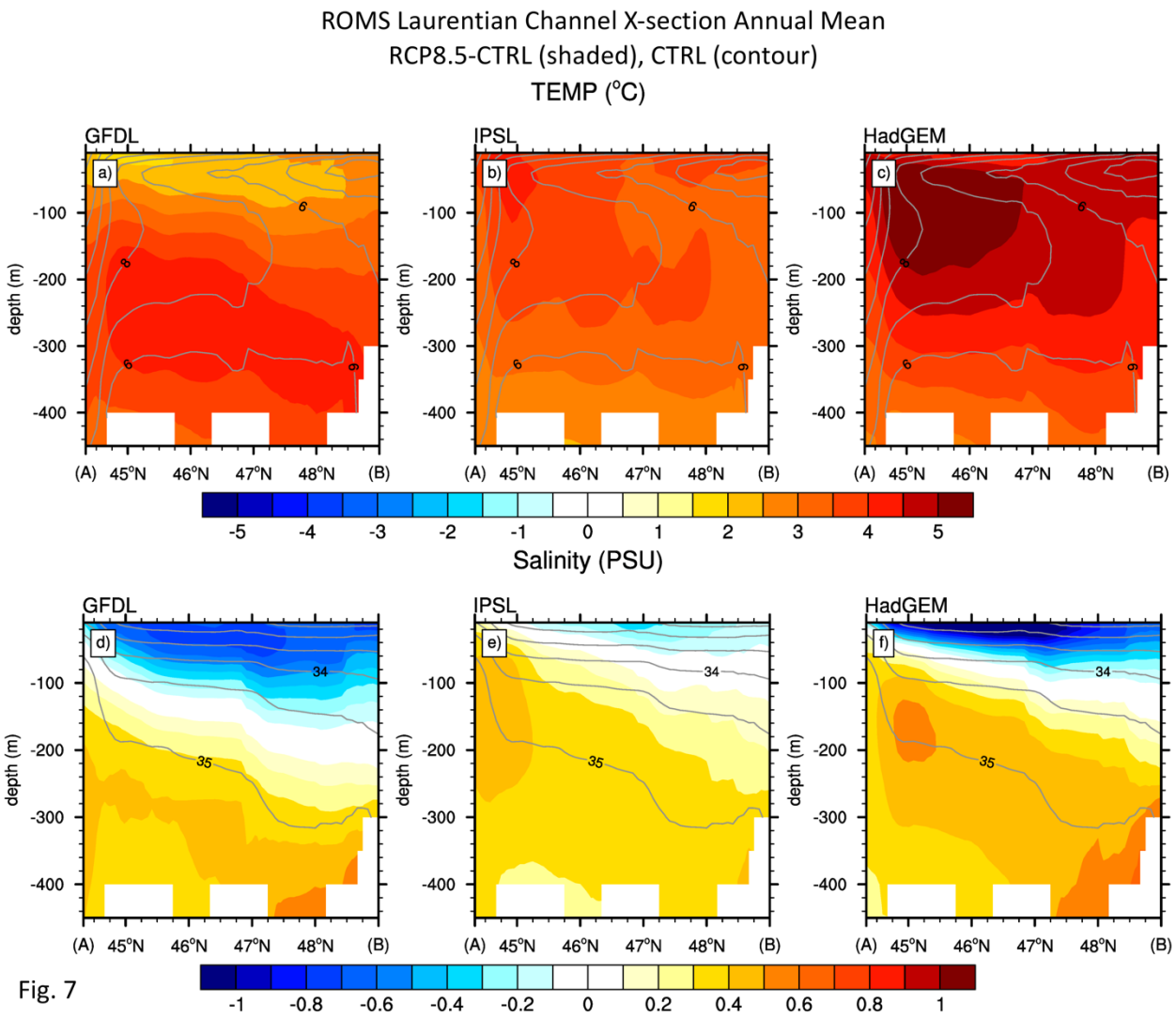

Fig. 7

Fig. 7. Cross section of the annual mean temperature (top) and salinity (bottom) along the Laurentian Channel in ROMS. Shown are the temperature from CTRL (contour, interval 1.0 ˚C) and the response (shaded, interval 0.5 ˚C) and salinity from the CTRL (contour, interval 0.5 PSU) and the response (shaded, interval 0.1 PSU) in (a) (d) GFDL-ROMS, (b) (e) IPSL-ROMS, and (c) (f) HadGEM -ROMS. Note the section is along the bottom of channel (not a straight line) and extends from the southeast to northwest, from (A) to (B) in Fig. 1.

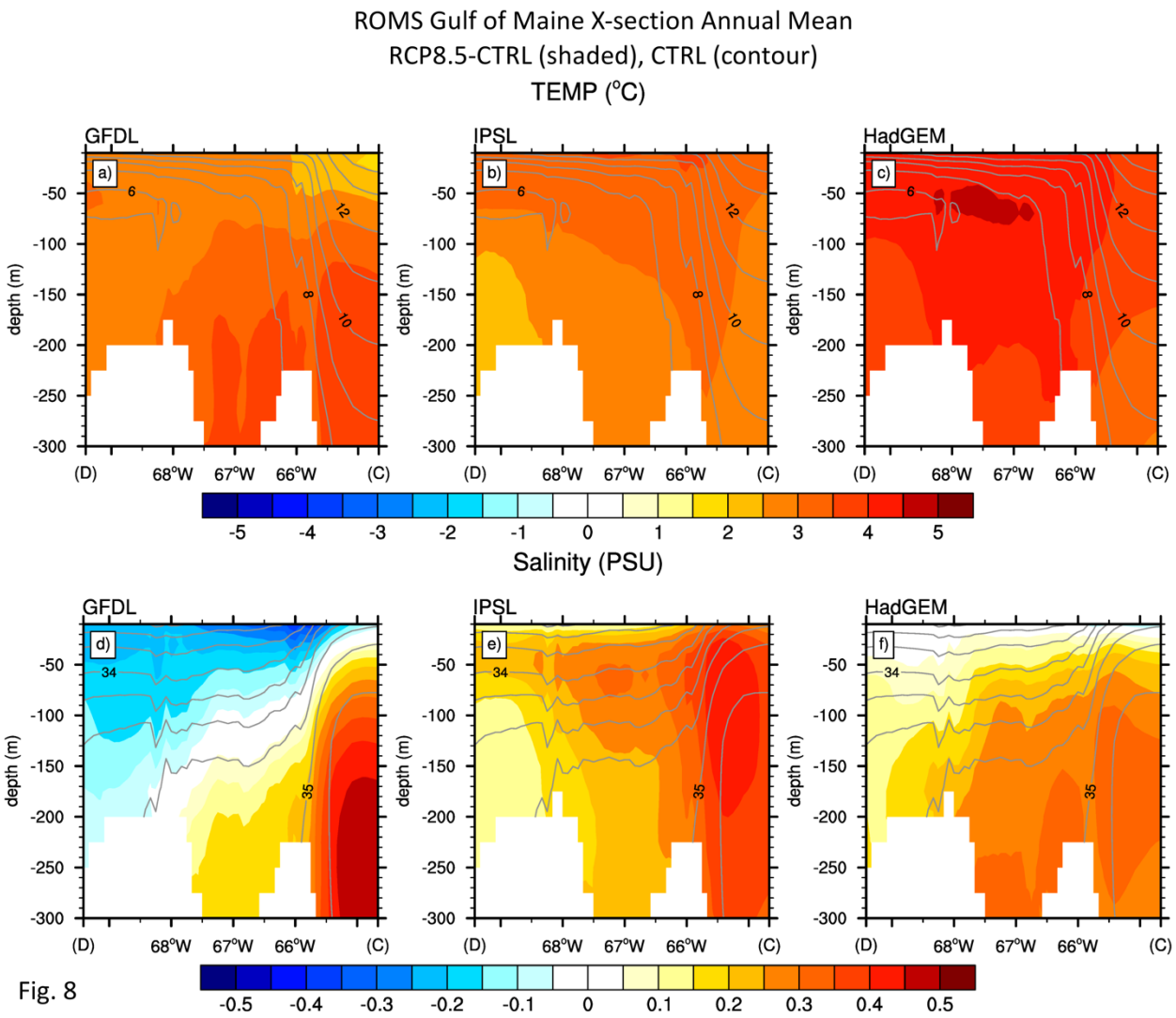

Fig. 8

Fig. 8. Cross section of the annual mean temperature (top) and salinity (bottom) into the Gulf of Maine in ROMS. Shown are the temperature from CTRL (contour, interval 1.0 ˚C) and the response (shaded, interval 0.5 ˚C) and salinity from the CTRL (contour, interval 0.25 PSU) and the response (shaded, interval 0.05 PSU) in (a) (d) GFDL-ROMS, (b) (e) IPSL-ROMS, and (c) (f) HadGEM-ROMS. Note the section is in the deepest part of the Gulf (not a straight line) and extends from east to west, from (C) to (D) in Fig. 1.

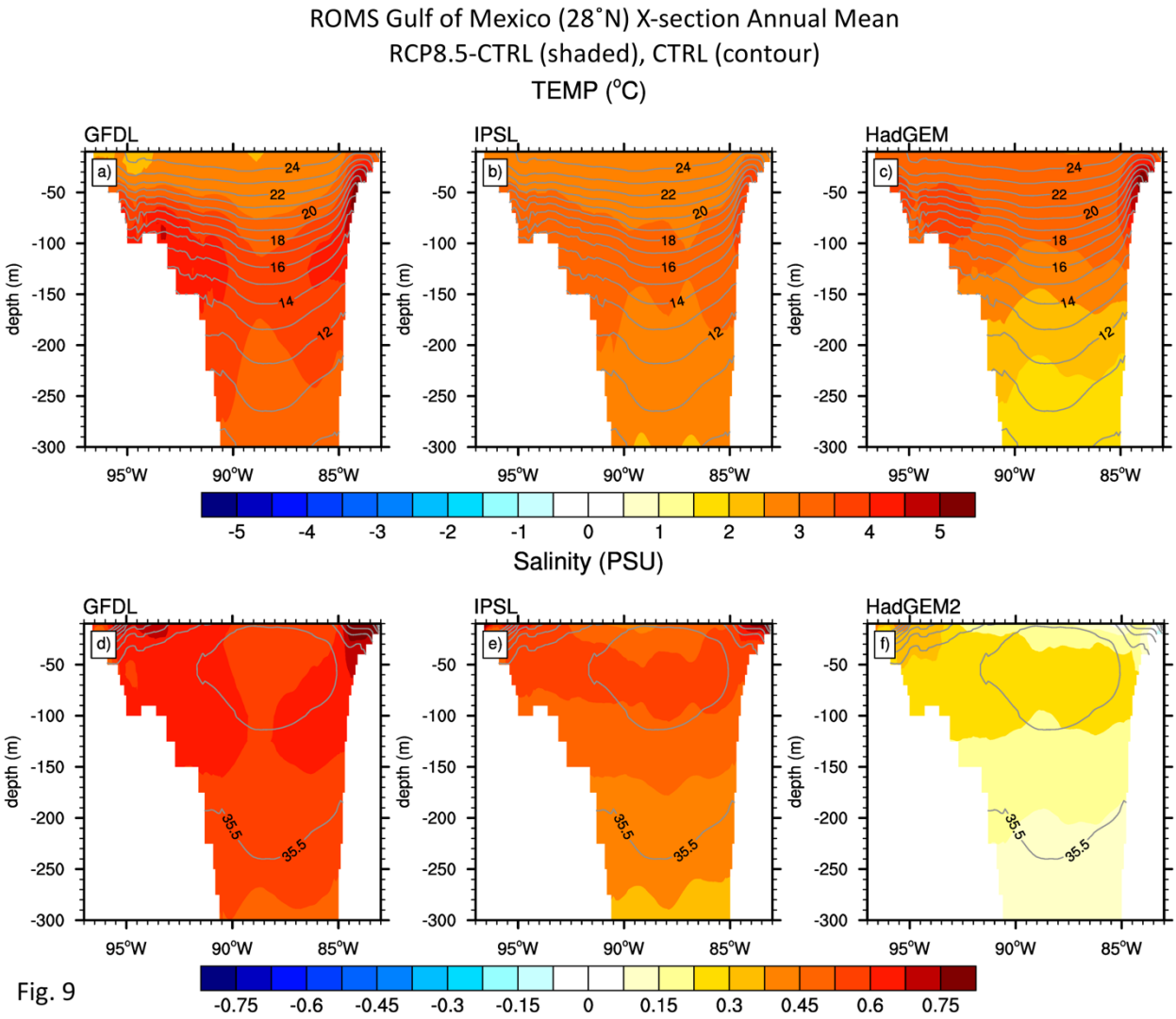

Fig. 9

Fig. 9. Cross section of the annual mean temperature (top) and salinity (bottom) along 28 ˚N in the Northern Gulf of Mexico in ROMS. Shown are the temperature from CTRL (contour, interval 1.0 ˚C) and the response (shaded, interval 0.5 ˚C) and salinity from the CTRL (contour, interval 0.5 PSU) and the response (shaded, interval 0.075 PSU) in (a) (d) GFDL-ROMS, (b) (e) IPSL-ROMS, and (c) (f) HadGEM-ROMS.

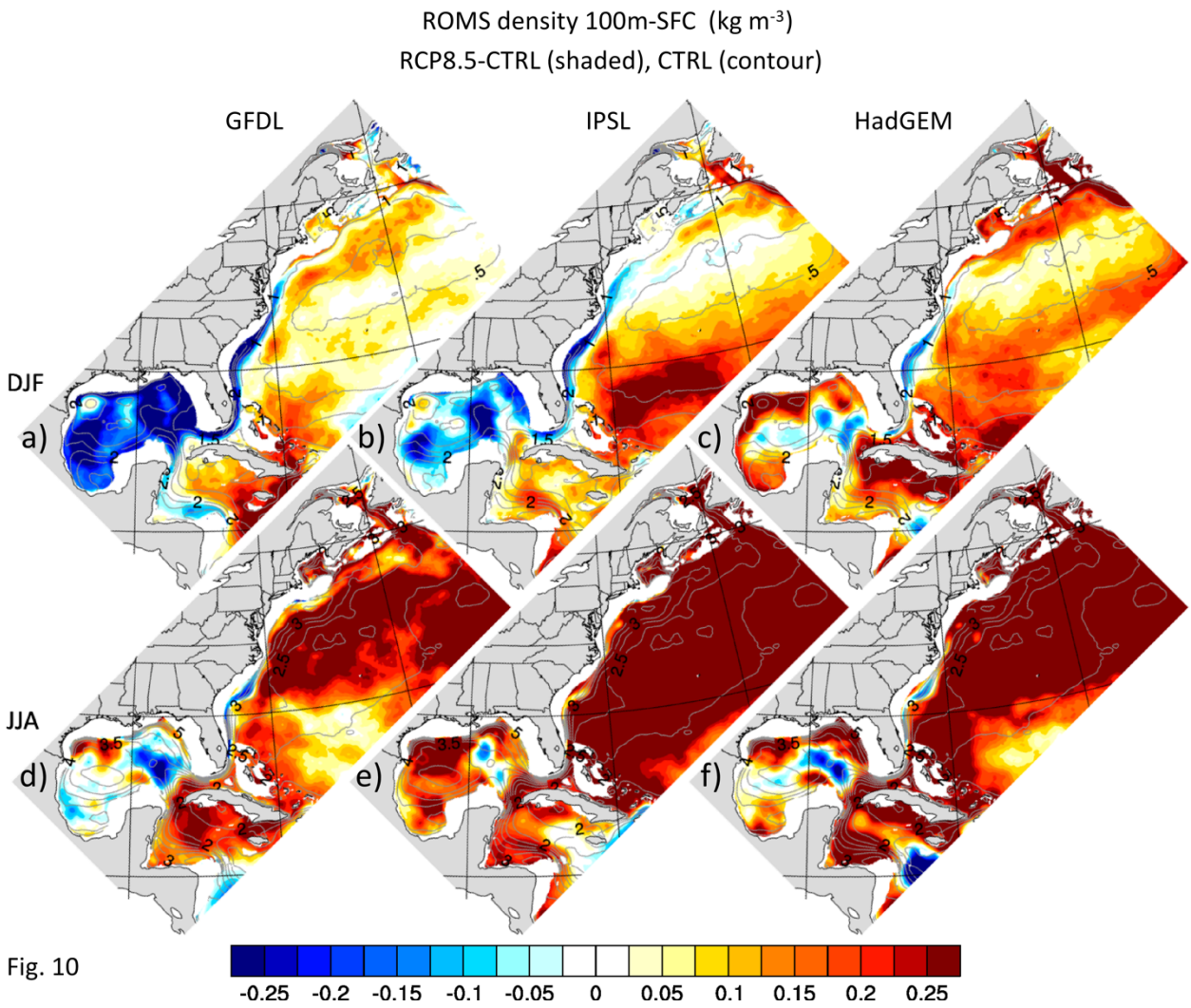

Fig. 10

Fig. 10. Static stability, derived from the density difference between 100 m and the surface, in the CTRL (contours, interval 0.25 kg m^{-3}) and the static stability response (RCP8.5-CTRL, shaded, interval 0.025 kg m^{-3}) in ROMS during DJF (top row) and JJA (bottom row) in (a) (d) GFDL-ROMS, (b) (e) IPSL-ROMS, and (c) (f) HadGEM-ROMS.

963

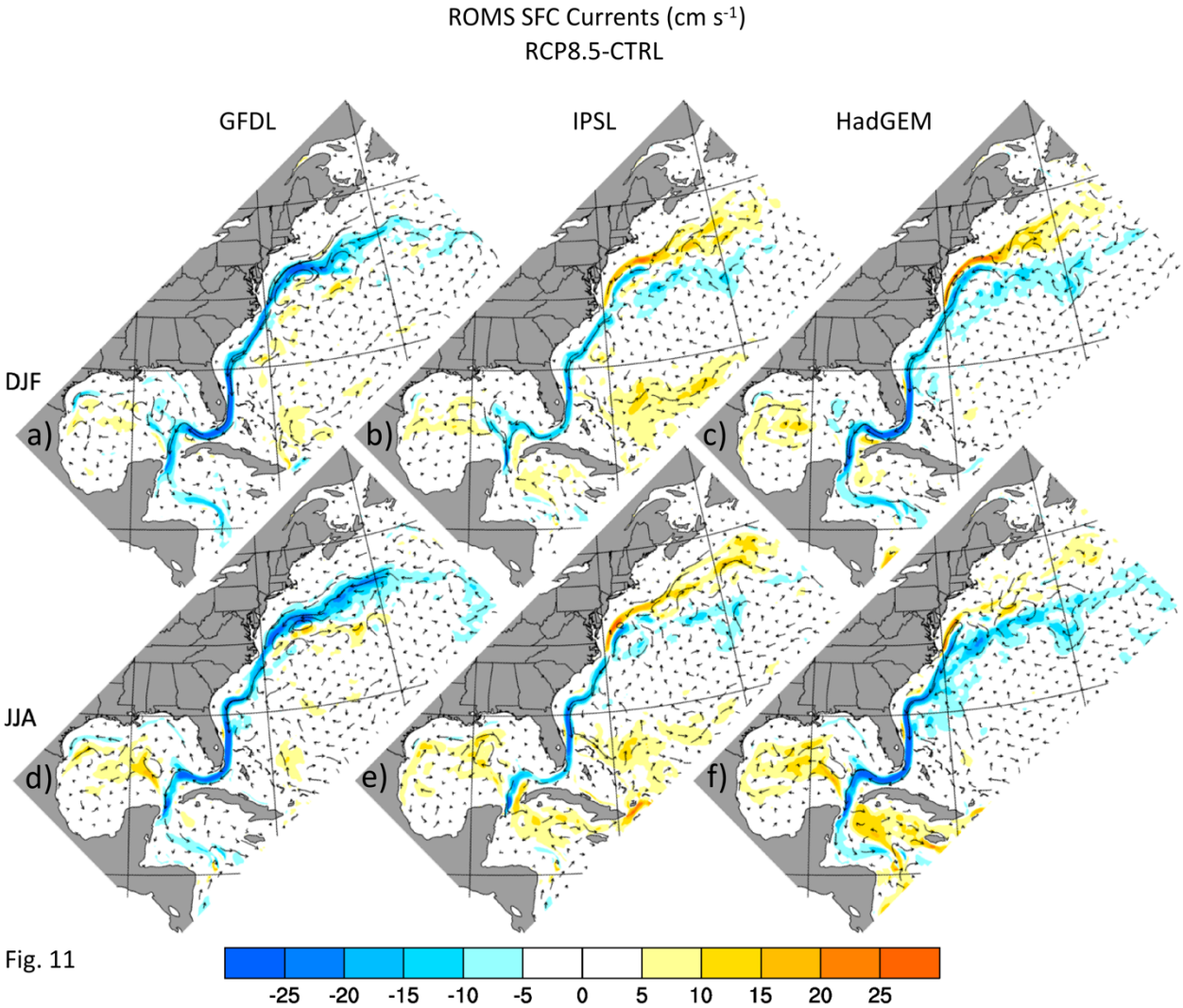

Fig. 11

964 Fig.11. Surface current response (RCP8.5 – CTRL, speed shown by shading, interval 5.0 cm
965 s^{-1}) in ROMS during DJF (top row) and JJA (bottom row) in (a) (d) GFDL-ROMS, (b) (e)
966 IPSL-ROMS, and (c) (f) HadGEM-ROMs.
967

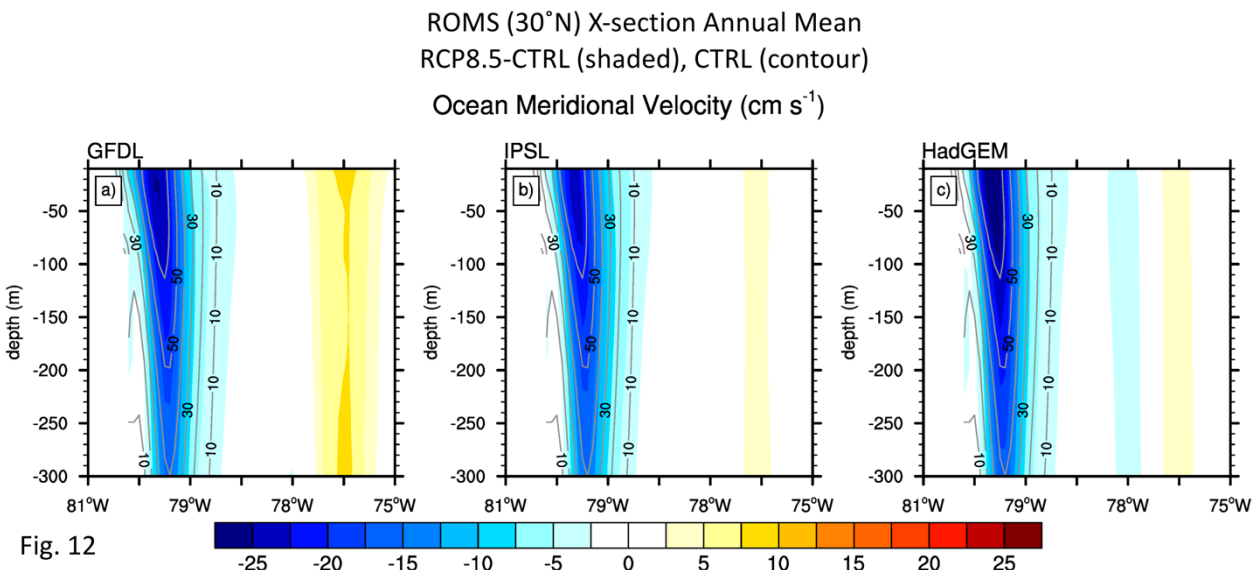

Fig. 12

Fig. 12. Cross section of the annual mean meridional velocity along 30˚N in the western North Atlantic in ROMS. Shown are the velocity from the CTRL (contours, interval 10 cm s^{-1}) and the response (RCP8.5 – CTRL, shading, interval 2.5 cm s^{-1}) in (a) (d) GFDL-ROMS, (b) (e) IPSL-ROMS, and (c) (f) HadGEM-ROMS.

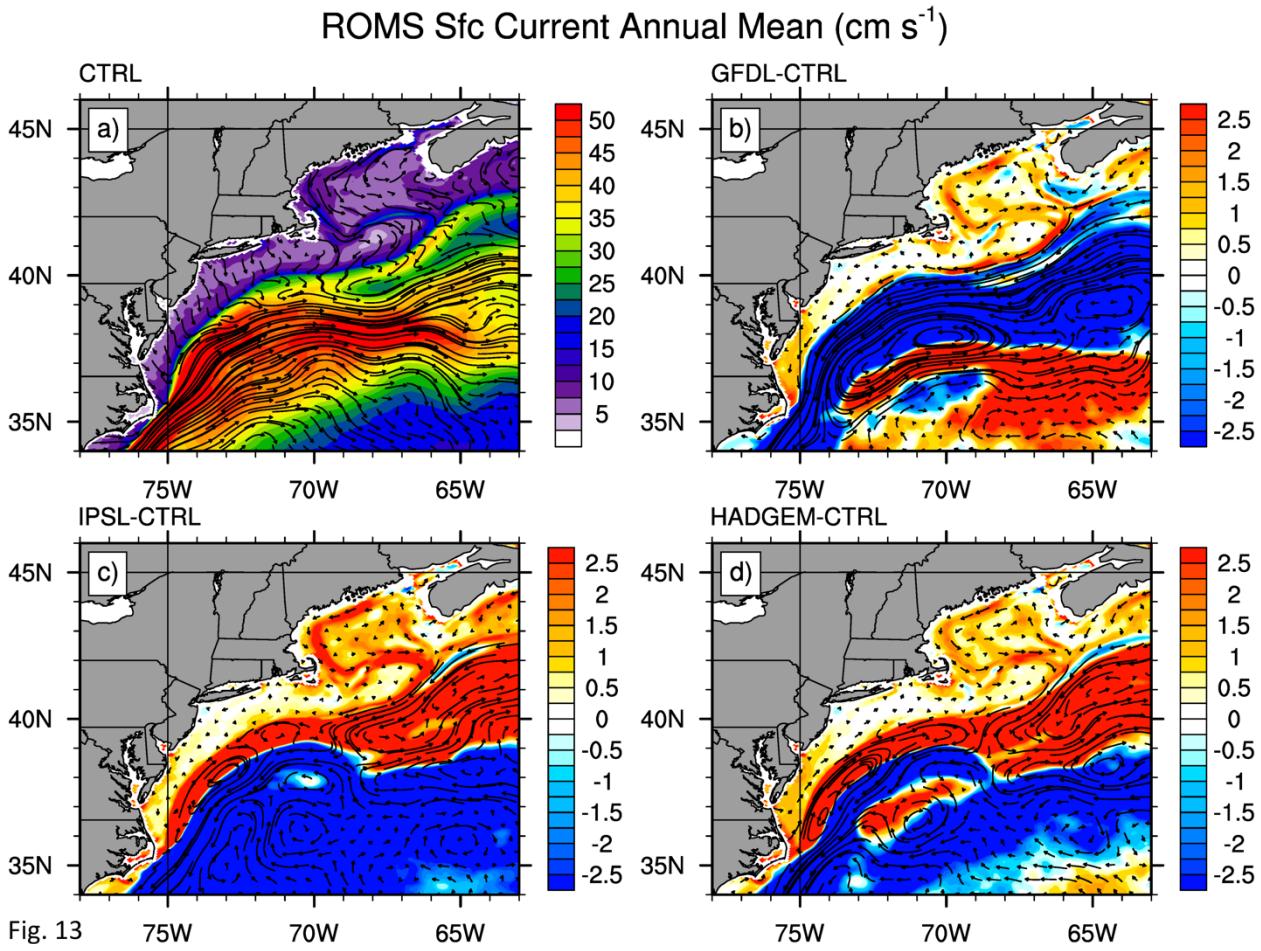

Fig. 13

Fig.13. Annual mean surface current off the northeast US coast in the (a) CTRL (2.5 cm s^{-1} shading interval), and the current response (RCP8.5 – CTRL, shaded, interval 0.25 cm s^{-1}) in (b) GFDL-ROMS, (c) IPSL-ROMS and (d) HadGEM-ROMS.

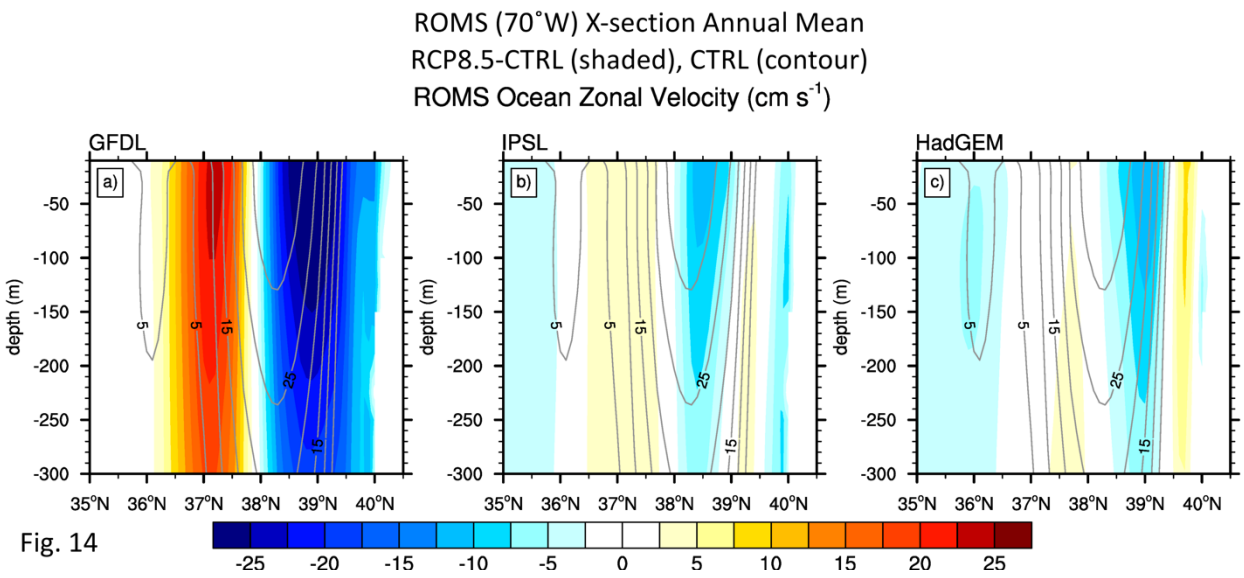

Fig. 14

Fig. 14. Cross section of the annual mean meridional velocity along 70˚W in the western North Atlantic in ROMS. Shown are the velocity from the CTRL (contours, interval 5 cm s^{-1}) and the response (RCP8.5 – CTRL, shading, interval 2.5 cm s^{-1}) in (a) GFDL-ROMS, (b) IPSL-ROMS, and (c) HadGEM-ROMS.

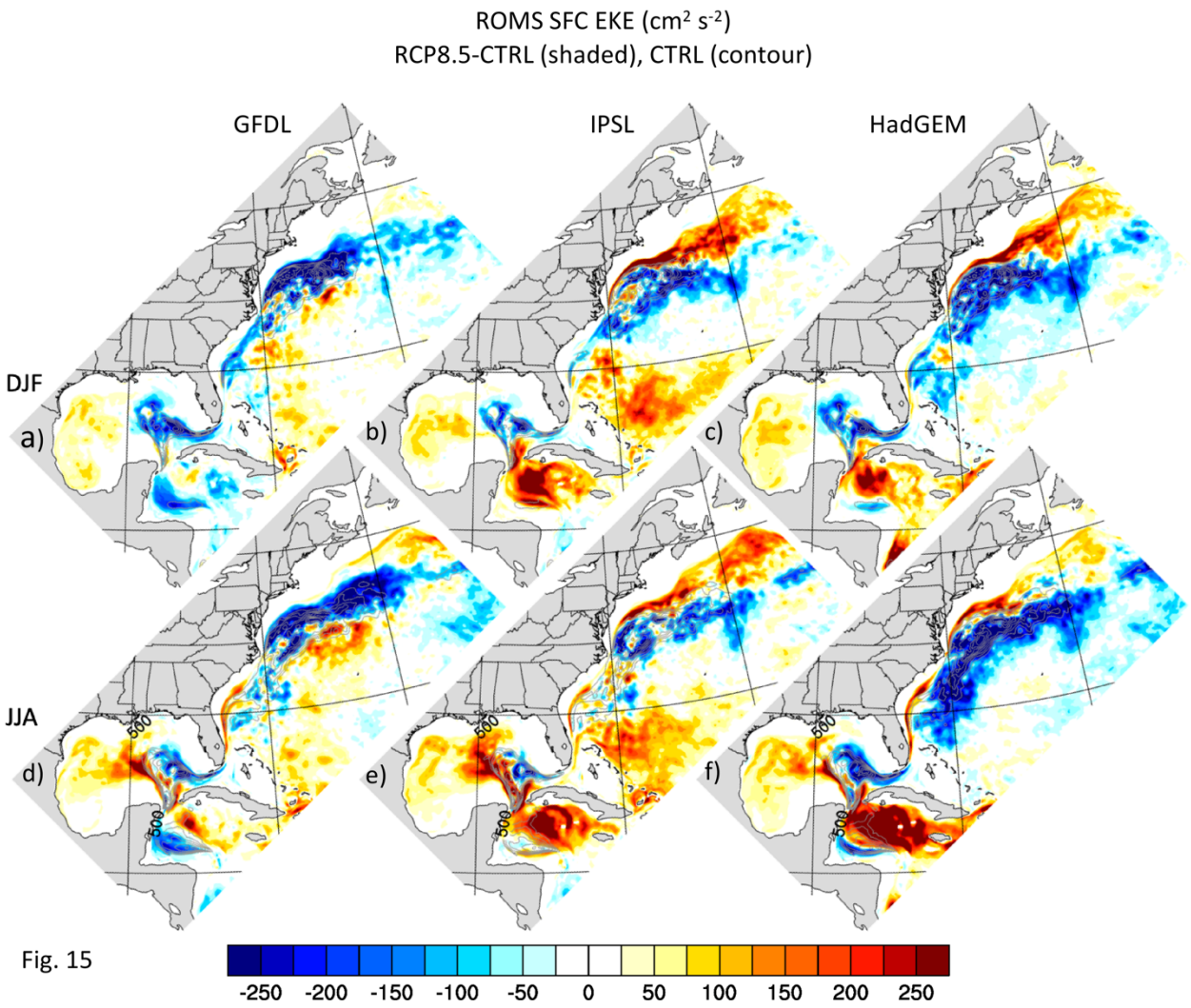

Fig. 15

Fig. 15. Surface eddy kinetic energy (EKE) in the CTRL (contours, interval 100 cm^2 s^{-2} starting at 500) and the EKE response (RCP8.5-CTRL, shaded, interval 25 cm^2 s^{-2}) in ROMS during DJF (top row) and JJA (bottom row) in(a) (d) GFDL-ROMS, (b) (e) IPSL-ROMS, and (c) (f) HadGEM-ROMS. The EKE is computed by removing 120-day running mean from the 5-day average velocity.